Hemodynamic Flow Characterization of St. Jude Medical Bileaflet Mechanical and Bioprosthetic Heart Valve Prostheses in a Left Ventricular Model via Digital Particle Image Velocimetry

Olga Pierrakos

Thesis submitted to the Faculty of the Virginia Polytechnic Institute and State University in partial fulfillment of the requirements for the degree of

Master of Science

in

Engineering Mechanics

Dr. Pavlos Vlachos, Chair

Dr. Demetri Telionis

Dr. Joel Berry

Dr. Lee Pyle

November 15, 2002

Blacksburg, VA

Keywords: Mechanical heart valves, orientation, St. Jude Medical, vorticity, turbulence, DPIV

Hemodynamic Flow Characterization of St. Jude Medical Bileaflet Mechanical and Bioprosthetic Heart Valve Prostheses in a Left-Ventricular Model via Digital Particle Image Velocimetry

Olga Pierrakos

(ABSTRACT)

The performance of the heart after a valve replacement operation will greatly depend on the flow character downstream the mitral valve thus a better understanding of the flow character is essential. Most in vitro studies of the flow downstream of a MHV have been conducted with the valve in the aortic position. Researchers reported detailed measurements most of which were obtained by Laser Doppler Velocimetry (LDV) in rigid models of the aorta. Digital Particle Image Velocimetry (DPIV) has also been utilized to reveal intricate patterns of interacting shed vortices downstream of the aortic valve. The orientation of the valves may considerably affect the flow development and slight difference may produce significant differences in the ventricular flow fields. Two orientations, respectively anatomical and anti-anatomical, of the St. Jude Medical (SJM) bileaflet valve are presented and compared with the SJM Biocor porcine valve, which served to more closely represent the natural valve. In this effort, we employ a powerful tool to monitor the velocity field in a flexible, transparent LV and study the evolution of large eddies and turbulence through a complete cardiovascular cycle. Both time average and instantaneous results of velocity, vorticity, and turbulent kinetic energy distributions are presented. The presence and location of vortical structures were deduced as well as the level of coherence of these structures. The presence of three distinct flow patterns were identified, by the location of vortical structures and level of coherence, for the three configurations corresponding to significant differences in the turbulence level distribution inside the LV.

TABLE OF CONTENTS

LIST OF FIGURES

ACKNOWLEDGMENTS

First and foremost, I would like to thank God for giving me the opportunity to reach this chapter of my life. Without God, I would not be where I am today for He has guided this path of mine. The support of my family, my friends, and my advisors, Dr. Pavlos Vlachos and Dr. Demetri Telionis, has been a constant reminder of achieving my goals, challenging myself, and growing each and every day. Without these individuals, who have shaped my life and influenced my being, I know that my life would not have taken the path that it has. I am so very grateful and honored!

Dr. Vlachos, Pavlo, truly no words can express how much you have taught me and how much you have influenced and molded my life. Your passion for research, but most importantly for life, has taught me to surpass and transcend myself. In my mind, you are a radiating light and a mentor for the rest of my life. You certainly never seize to amaze me. Thank you for your encouraging words and your support. Thank you for believing in me and challenging me to grow every step of the way. I am forever grateful and privileged to have walked beside you. However, I am not done learning from you!

Dr. Telionis, whose optimism and aspiration has allowed me to be here, I thank you so much. You exude such warmth and kindness. I am astonished everyday by the power of your mind. You are an inspiration to me. I thank you for your words of advice and your sensuous character that I respect and admire.

I would also like to thank my other committee members, Dr. Joel Berry and Dr. Lee Pyle. Dr. Berry, your words of affirmation have helped me so much more than you can imagine, thank you for believing in me. Dr. Pyle, you introduced us to the clinical aspect of biomedical engineering, I am thankful for your continual support.

Without my friends in the lab, I can't imagine where I would be today. Thank you Saami Yazdani (Yaz) for showing and reemphasizing the meaning of what a true friend really is. Thank you Ali Etebari for your optimistic attitude and always so generous character. Thank you Amber

Mace for all your support and encouraging words. Thank you Claude Abiven for making me challenge myself and helping me grow as a person. Thank you Roger Chang for being such a great friend. Thank you Yingzhi for all your help. To all the people in the Fluid Mechanics Lab, I am honored to work with you. You are all amazing and I am honored to say that I am your friend and colleague.

To my family who has shown me so much love and support, I love you with all my heart. My parents have been an inspiration to me and serve as a constant reminder of who I am today. My father's philosophic insight has allowed me to face and question life and our purpose as individuals. My mother, who I respect and admire so much, has taught me to be a fighter and to persevere through anything and everything. The kindness of your heart and soul is immeasurable. To my parents, thank you for believing in me and for all your inspiring words. To my sister, Nayia, and my two brothers, Diamadi and Dino, thank you for your support. To my sister who I have always adored, thank you for your understanding, kindness, and compassion. To my brother Diamadi, your unselfish and genuine character has taught me so much, thank you for being so amazing. To my brother Dino, you are certainly one of a kind, thank you for your kindheartedness and support. Also, I would like to thank my Aunt Chrisoula and my grandmother, who have shaped my life in such a unique way. You are inspirations in my life and I admire you both so much. Thank you for the all so many lessons about life. John Karabelas, Yianni, thank you for your patience and your love. The kindness of your heart is unending, you are remarkable. Thank you for your support.

Dedicated to My Loving Family

With Much Love and Adoration

CHAPTER 1

1 BACKGROUND AND INTRODUCTION

1.1 Motivation

Although mechanical heart valves (MHV) have evolved to a level of universal acceptance, they have never reached a level of performance comparable to that of the natural valves of the heart. Consequently, MHV implantation is not always an ideal solution. There is a continual obligation to better understand the mechanical behavior of MHVs, in vitro and in vivo, to study the effects and presence of thrombosis, hemolysis, cavitation, transvalvular pressure fluctuations, high levels of shear stress and certainly the association and interaction of all these conditions. Apparently, the flow through pivoted leaflets of MHVs induces a combination of flow characteristics, which are clearly dependent on the specific valve design and orientation that could result to many pathological conditions. All these conditions reduce the efficiency of the heart, being in a state far from natural.

Clinical practice has demonstrated that the orientation of MHVs greatly affects the postoperative performance of the left ventricle (LV). Previous studies attempted to document the dependence of the left ventricular performance on valve orientation; however, the underlying physical principles are yet not clearly understood. The motivation of this present study is to provide new insight on the spatio-temporal character of the flow distal to a mitral MHV and further support the hypothesis that the appropriate orientation of MHVs can improve the hemodynamic performance of the LV. This effort of exploring the function and hemodynamic parameters of mechanical valves could lead to a better understanding of artificial elements and

therefore guide the surgeon and the supporting scientists in their efforts to improve the clinical procedure and the prosthetic hardware. It is also possible that this effort may guide researchers in developing new prosthetic devices or new diagnostic techniques.

1.2 Background

The second most common major heart operation in the western world is valve replacement surgery. Cardiac valves are intended to fully replace a diseased natural valve and their replacement has been an established clinical practice for more than four decades. Today over 100,000 valves are replaced worldwide per year. The most commonly replaced valves are the mitral and aortic valves due to the higher pressure loads on the left atrium and left ventricle of the heart. Any of the four valves can become either too leaky (regurgitant), or too tight (stenotic). Figure 1.1 shows the anatomy of the heart and the location of each of the four heart valves.

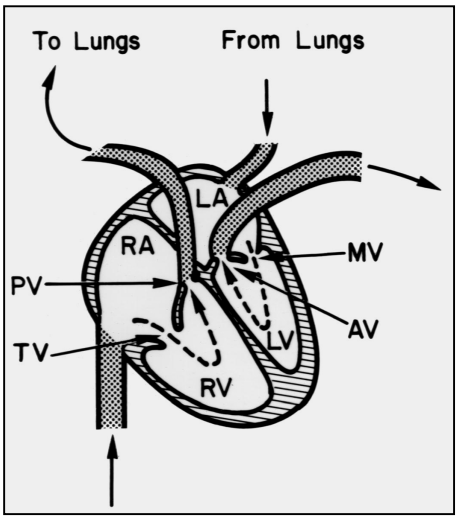

Figure 1.1: Simple schematic of the heart anatomy.

Regurgitant valves stress the heart by allowing the blood to flow partly backward forcing the heart to pump harder in order to circulate enough blood throughout the body. Stenotic valves stress the heart by resisting the normal forward flow of blood resulting in blood back up behind the valve. These two problems reduce the efficiency of the heart and create a jet of blood that impinges on the inner walls producing a high-pressure system leading to permanent damage. The two major problems related to the blood flow are thrombus formation and hemolysis, which damages red blood cells. It is well known that the shear stress in the fluid and flow separation around the valve are blamed for such disastrous phenomena (Shim, 1997); therefore, it is obvious that there is a need for more effective artificial heart valves to be designed to prevent these types of situations from occurring.

1.2.1 Artificial Heart Valve (AHV) Prostheses

Cardiac valves are subjected to a large number of cycles, about 35 million per year. A typical functional life of an artificial valve is ten years, although a valve can last up to 30 years in some patients. In 1952, the first artificial heart valve was implanted and since then, many advances have been made in heart valve design. Many different types of artificial heart valves have been devised over the years. The advantages of biological valves are their hemodynamic performance, which is very similar to human valves, and their lack of anticoagulant use. The major disadvantage is their short life span, 5-7 years, which is why they are less suitable for younger patients. Mechanical valves were invented by the need for a long lasting valve with reduced risks of calcification. On the other hand, mechanical valves damage red blood cells more than tissue valves do, and they tend to cause the formation of blood clots. The first successful mechanical valve replacement occurred in 1960 with an open caged-ball valve. This valve offered a dependable alternative to bioprostheses but still produced calcification around the valve. This brought about the tilting-disc valve in 1967 followed bileaflet in 1976, which is the most popular valve used today. New prosthetic valve designs are designed to improve structural durability and hemodynamic

performance. Although, biological valves have a better performance, the most commonly implanted artificial heart valve is the bileaflet mechanical valve, which is the design that was studied in this study, specifically the St. Jude Medical bileaflet mechanical valve.

1.2.2 Modeling the Left Ventricle

A model is designed to simulate a complicated physical phenomenon in order to understand its behavior in a more simplistic manner. In some cases, the models are too complex to be of practical use, while others are too simple to yield useful results. An accurate design of a testing system that replicates true body conditions is vital and will assist with research on improvements in design and testing of prosthetic valves. The testing of artificial heart valves and investigation of flow characteristics in a physiologically accurate simulation of the human heart is essential considering that it could lead to innovations in valve designs or modifications to the currently available designs.

In modeling ventricular behavior, the shape of the cavity and the thickness of the wall have to be considered as well as the muscle behavior. Many, including Beneken in 1965, approximated the left ventricular wall by a spherical shell and the right ventricular free wall as a thinner spherical shell wrapped around part of the outer surface of the thick-walled left ventricle (Bergel, 1972). The cylindrical and spherical approximations of the left ventricle also assume a homogeneous isotropic wall material; however, the wall of the ventricle is composed of muscle fibers, which have a very specific directional distribution. According to Sonnenblick, "since the ventricular myocardial fibers contract sequentially, the strength of contraction of the later-contracting myocardial fibers is influenced by the strength, the rate, and the sequence of contraction of the fibers that contract earlier and that stretch the later-contracting fibers" (1994). Each contraction of the heart is initiated by an electrical event that occurs because cardiac muscle is an excitable tissue. It is important to review the major principles of muscle mechanics relevant to the study of myocardial function, and

to provide a basis for the critical evaluation of methods for the description and measurement of the contractile performance of heart muscle.

With that in mind, very little has been done to explore the flow inside ventricular chambers and so far, most studies have been carried out using rigid ventricle models. In this experimental effort, a geometrically similar silicone ventricular model was utilized with uniform thickness of 2-mm. The model is transparent and flexible.

1.2.3 Analogous Blood Fluids

Despite the fact that blood in a non-Newtonian fluid, model fluids with Newtonian rheological properties are used in most cases to test and study the performance of artificial heart valves in vitro. From the literature, the most common blood analog fluids used fluids are water and simple glycerol solutions. In the present study, water was used.

1.3 Testing Techniques

Several efforts have been made to test artificial heart valves taking into account the above information as knowledge for the simulation models. Different experimental methods have been developed to investigate the flow through artificial heart valves and also test the effectiveness of their design. Some systems consist of a piston-in-cylinder pump head driven by a low inertia electric current, the bellows/swash plate technique, a transparent ventricular sac, and computer models. In all these efforts to solve the problem of testing artificial heart valves, it is important to understand biofluid dynamics as it pertains to designing any sort of artificial organ including total

hearts, vascular grafts, and certainly heart valves. In one example, good flow characteristics must be designed to reduce fluid friction losses and minimize flow-related damage to tissues and cells.

1.3.1 Computational Testing Techniques

According to Bergel, "Warner (1959) published a computer model of the cardiovascular system in which he represented the action of the heart by time-varying compliances" (1972). Since then, many others have used the same principle, which is attractive because the time course and amplitude of the compliance can be changed easily (Bergel, 1972). For the past two decades, computational fluid dynamics has been a useful tool in the study of cardiovascular fluid mechanics. Several groups developed models to simulate steady laminar flow through a two-dimensional rigid heart valve. As the available technology expanded, so did the complexity of the computer models. By the late 1980s, it was feasible to simulate three-dimensional time-dependent flow, such as that occurring in a heart (Yoganathan, 1994). The computer-generated left ventricle and aorta were surfaces represented as a set of points. This study showed that the thin-walled three-dimensional left ventricular computer model gave a realistic picture of normal left ventricular function. According to Yoganathan and his colleagues, "the computer left ventricle was compliant (i.e., all the structures were free to move in response to fluid forces), agreement between the model and the native heart on structural motion would indicate that the forces altering the computational structure were physiologic" (Yoganathan, 1994). Yoganathan's algorithm is limited to simulated flows with a local cell Reynolds number of two or less. Therefore, it was necessary to approximate the intraventricular blood flow as a low Reynolds number flow. While this approximation is valid for early systole, it is impossible that the model could accurately simulate peak or late systolic flow fields. According to Bluestein, "the presence of turbulence in the cardiovascular system is generally an indication of some type of abnormality" (Bluestein, 1994). Most cardiologists agree that turbulence near a valve indicates either valvular stenosis or regurgitation, which could lead to an artificial heart valve implant. Accompanying mitral valve closure is unsteady flow, which goes

against the computational design, allowing only laminar steady flow leading to unrealistic results. This turbulence also implies higher Reynolds numbers, therefore, making the computer heart model inadequate.

1.3.2 Experimental Testing Techniques

Only as recently as 1996, in vitro flow visualization studies have focused on understanding the flow characteristics through prosthetic heart valves. Many mature visualization techniques such as particle methods have been applied to study prosthetic valve flow patterns under steady and pulsatile flow conditions. Recent flow visualization applications have addressed the flow patterns generated by bioprosthetic and mechanical heart valves in both the mitral and aortic positions as well as in rigid and flexible models.

Most in vitro studies of the flow downstream of a MHV have been conducted with the valve in the aortic position (Chandran et al. 1983, Chandran et al. 1985, Reul et al. 1986, Bruss et al. 1983, Giersiepen et al. 1986, Yoganathan et al.1986, Hasenkam et al. 1988, Hanle et al. 1989, Giersiepen 1989, Tonietto 1990, Lim et al.1994). In vitro experimental studies of the flow downstream of a MHV in the mitral position are fewer and more complicated due to the dynamically changing LV geometry. Initial studies simplified the problem by employing rigid models of ventricles (Woo and Yoganathan 1986, Chandran et al. 1989, Schoephoerster et al. 1993). Chandran et al. (1989) and Schoephoerster et al. (1991) employed more realistic rigid ventricular models. Garitey et al., (1995) also employed a flexible sack model of the LV, made extensive pressure measurements and used pulsed ultrasound Doppler Velocimetry to record in detail the velocity field. They captured the activity of vortical structures in the ventricular chamber and compared the effects of three MHVs and their orientation when mounted on their model. They found that slight differences in the valve design may produce significant differences in the ventricular flow fields, thereby inducing large flow oscillations near the apex. Shortland et al. (1996) investigated the development of vortices in ventricle filling and their effect on the mitral valve

closure. Bellhouse and his co-workers have investigated ventricle filling and the effect of the vortices that develop and return to interact with the mitral valve as early as 1969 (Bellhouse 1969 and Bellhouse 1972). This study was followed by many other researchers (Lee and Talbot 1979, Reul et al.1981, Takatsusi et al 1996, Iwase et al. 2001). Bluestein et al., (2000) used a numerical simulation and Digital Particle Image Velocimetry (DPIV) to reveal intricate patterns of interacting shed vortices downstream of the aortic valve and demonstrated that blood elements exposed to the highest shear stresses in the immediate proximity of the MHV could be trapped within the vortices that form in the wake of the valve.

Experimental studies of the flow downstream of a MHV in the mitral configuration are more difficult, because of the continuously changing ventricle geometry. To simplify the problem and eliminate the difficulties of compliant walls, studies were first carried out employing rigid models of atria and ventricles. Woo and Yoganathan (1986) used rigid cylindrical models of both the left atrium and ventricle. Chandran et al. (1989) and later Schoephoerster et al.(1991) employed a more realistic ventricular configuration and an elastic atrium but were still limited to solid walls. In all these studies, Laser Doppler Velocimetry (LDV) was used to monitor the velocity field.

Recently (Kilner et al. 2000) employed magnetic resonance velocity mapping to study the streaming of blood flow in atrial and ventricular cavities. Their most intriguing conclusion was that the geometrical arrangements of the atria and the ventricles redirect the flow with sinous, chirally asymmetric paths, thereby minimizing dissipative interaction between entering, recirculating and outflowing streams. Figure 1.2 below, a schematic of what is seen from MRI images obtained from Laas's group in Germany (2000), serves to illustrate this phenomenon in the natural heart where smooth redirection of the flow is evident. The implication of Kilner's work is significant, as it appears to show that the heart pumps blood with minimum loss of energy. The wake of MHV leaflets during the deceleration phase has revealed an intricate pattern of interacting shed vortices (Bluestein et al., 2000). We shall see the importance of visualizing such highly structured patterns of vortices serving to provide a better understanding of the hemodynamic characteristics inside the LV.

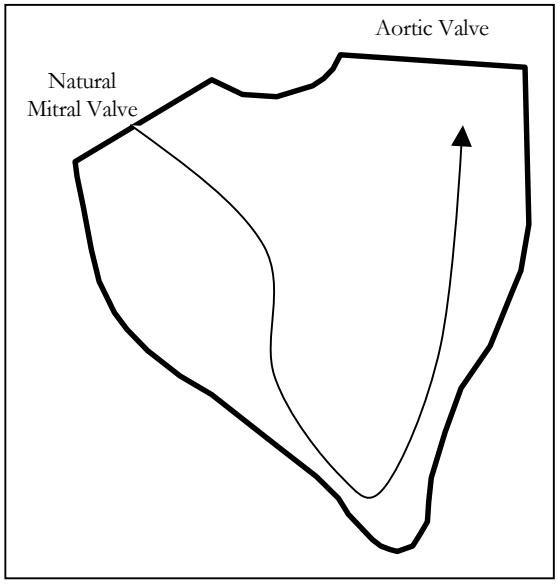

Figure 1.2: Schematic of the flow inside the left ventricle through the natural mitral valve as seen from MRI images.

1.3.3 Mechanical Heart Valve Orientation

According to Chandran et al. (1989), the geometry of the valve prostheses as well as the orientation of the valves may significantly affect the flow development including vortex formation, regions of stasis and disturbed flow in the LV. The wake of the valve is influenced by orientation, whether this includes tilting of the valve or simply rotation. The latter of the two is the focus of this study, which serves as an important parameter that needs considerable attention. Garitey et al., (1995), employed a flexible sack model of the LV and used pulsed ultrasound Doppler Velocimetry to record the velocity field, captured the activity of vortical structures and compared the effects of three MHVs and their orientation when mounted on their model. They found that slight differences in the valve design might produce significant differences in the ventricular flow fields, thereby inducing large flow oscillations near the apex.

Orientation of the aortic valve has been studied by Kleine et al. (1999) revealing that St. Jude Medical (SJM) valves showed lower turbulence and HITS (High-Intensity Transient Signals) counts in their hemodynamically best orientations. Also, Laas et al. (1999) showed that the optimal orientation of the SJM bileaflet valve in the aortic position was achieved when one leaflet was directed toward the right cusp. In contrast, fewer studies of bileaflet valve orientations in the mitral position have been performed. Chandran et al. (1989) performed transvalvular pressure and regurgitation measurements along with qualitative flow visualization. The two orientations studied were respectively (1) with the tilt axis parallel to the septal wall and (2) with the tilt axis perpendicular to the septal wall. The more favorable of the two was the second orientation because it offered a smoother washout of the fluid near the left ventricular free wall. Flow visualizations provided a qualitative representation of the flow patterns; however, the lack of global quantitative results limited the study. Fontaine et al. (1996) utilized pulsed wave Doppler velocity measurements, 2-D echocardiography, and selected color Doppler flow mapping to show that the SJM bileaflet valve oriented in the anti-anatomical position with chordal preservations is favored over tilting disc, porcine bioprosthetic, and pericardial bioprosthetic valves. Despite the fact that these two studies revealed the importance of valve orientation, both were limited to rigid LV models. The first study employed a geometrically similar LV model, while the second, even more constrained, utilized a rectangular LV.

The flow downstream of a bi-leaflet MHV is characterized by the formation and interaction of three jets during the systolic part of the cycle and their entrainment in an asymmetric sudden expansion area. Figure 1.3, which is a schematic of the flow as seen in MRI images obtained from Laas's group in Germany (2000), serves to show the dispersed outward flow generated inside the left ventricle by the three inlet jets of the bileaflet mechanical valve. The complexity of the geometry combined with the pulsatile character of the flow, the interaction of the jets with the LV flexible walls and the unsteady motion of the leaflets generate intrinsically complicated turbulent flow structures. As a result, conventional, time averaged or point measurement methods would fail to reveal the underlying character of the flow demonstrating the need for global, time resolved measurement techniques.

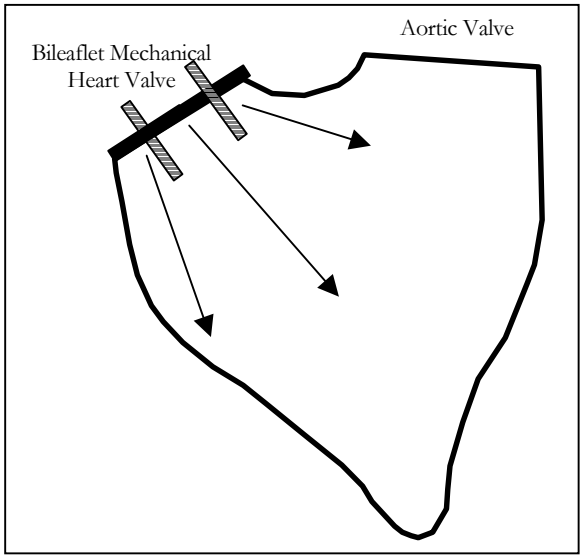

Figure 1.3: Schematic of flow inside the left ventricle through a mechanical bileaflet mitral valve as seen in MRI images.

1.4 Contribution

The complexity of the geometry combined with the pulsatile character of the flow, the interaction of the jets with the LV flexible walls and the unsteady motion of the leaflets generate intrinsically complicated turbulent flow structures. As a result, conventional, time averaged or point measurement methods, such as the ones employed in previous studies, would fail to reveal the underlying character of the flow demonstrating the need for global, time resolved measurement techniques. In this effort, time resolved Digital Particle Image Velocimetry (DPIV) results in a flexible, transparent LV are presented and the evolution of large eddies and turbulence during a complete cardiovascular cycle is investigated. Two mechanical orientations of the SJM bileaflet valve, to be discussed in more detail in Chapter 2, in the mitral position were studied along with the SJM Biocor biological valve, serving as our reference case. The state-of-the art DPIV system employed for the present study provides unsurpassed detail, which combined with an overall unparalleled experimental setup, gives rise to unique results.

Chapter 2

2 METHODS AND FACILITIES

Testing and research of artificial heart valves has involved in vivo and in vitro techniques. Due to the obvious difficulties pertaining to in vivo methods, in vitro techniques involve experimental and computational models. For example, point velocity measurement techniques such as Laser Doppler Velocimetry (LDV), which have been extensively used in the past, require a repeatable triggering event in order to reconstruct in a statistical sense the instantaneous character of pulsatile flow fields. In the present study, we bypass such difficulties by employing a novel time resolved Digital Particle Image Velocimetry (DPIV) system. The unique non-intrusive tool, DPIV, provides unsteady global field measurements of the flow in a planar sense. According to Yoganathan, "Studies demonstrating the full power and accuracy of PIV in pulsatile flow have yet to be presented" (1998). The methods and facilities utilized in the present study are described below. Specifically, we will start with a description of the heart simulator and prosthetic valve designs and end with details of DPIV and the corresponding hardware.

2.1 Heart Simulator

In studying the hemodynamic characteristics through artificial heart valves and the left-ventricular model, a simulation machine shown in Figure 2.1 was constructed. Similar machines have been constructed and operated in the past (Reul et al.(1981), Gross et al.(1988), Giersiepen et al. (1989), Garitey et al., (1995), Shortland et al. (1996) Liu et al. (1996), and Mouret et al. (2000). A flexible transparent silicone sack simulates the left ventricle and allows for optical access as a transparent model fluid is used to simulate blood, in our case water. A rectangular tank with

transparent walls houses the left ventricular model and also allows for optical access. Index of refraction matching is taken into account, thus minimizing any optical distortion induced by curved walls. A piston with adjustable travel on the side of this tank dynamically controls the stroke volume of the LV model and consequently also the ejection fraction. These tasks are driven by a motor with variable frequency which, in turn, allows for fluctuations of the heart rate (beats per minute). The systolic and diastolic pressure at the exit and entrance of the LV are hydrostatically controlled and can be adjusted by the user. Specifically, the simulation of pressures is achieved by controlling the elevation of the delivery and the receiving tanks, which can be though as representing the left atrium and aorta respectively.

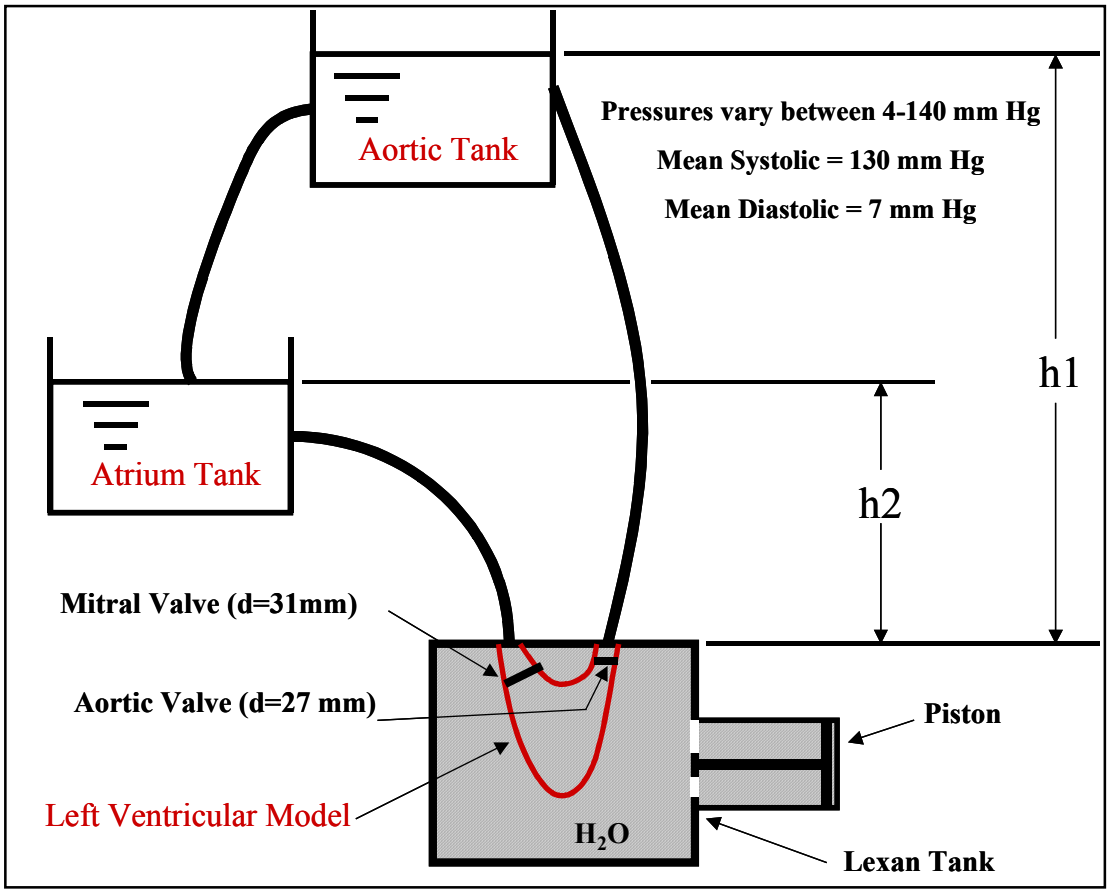

Figure 2.1: Simple schematic of heart simulator.

The machine simulates the operation of a ventricle as follows. When the piston forces more fluid in the tank, the sack is compressed, simulating the systolic phase of the motion. The mitral valve is closed and the aortic valve opens and allows the flow into the receiving tank acting as the aorta, working against the head of the upper tank that simulates the systolic pressure. When the piston is withdrawn, the sack expands and the diastolic phase of the motion is initiated. This, of course, is a simplification of the systolic motion induced by the heart muscles. The actual motion of the heart is not uniform. True systolic action is initiated from the apex and extends gradually upward with some twisting or torsion affects as well. It is not known whether these motions affect the fluid mechanics of the interior of the ventricle although pressure and flow rate measurements have been extensively carried out to ensure the operational repeatability of the heart simulator. For the present experiments, the simulator was operated at 1-Hz, an average stroke volume of 95-mL, and a mean Reynolds number of 2700 based on the mitral valve diameter of 31 mm.

2.2 St. Jude Medical Bileaflet Mechanical Heart Valve

According to St. Jude Medical (SJM), the basic design of the SJM mechanical heart valve has remained virtually unchanged in the 23+ years since its first use. The valve, shown in Figure 2.2, is designed and manufactured of pyrolytic carbon and is tungsten impregnated. In the present study, St. Jude Medical bileaflet mechanical valves were studied and placed in the mitral and aortic positions. The orientation of the valve was changed for the mitral valve only. The two positions studied corresponded to the anatomical and anti-anatomical orientations as shown in Figure 2.3, which are with respect to the plane defined by the centerlines of the natural valve leaflets and the septal wall. More specifically, in the anatomical position, the leaflets of the MHV open parallel to the natural heart valve while in the anti-anatomical orientation, the leaflets open in an angle of 90° with respect to the latter.

Figure 2.2: St. Jude Medical mechanical bileaflet heart valve.

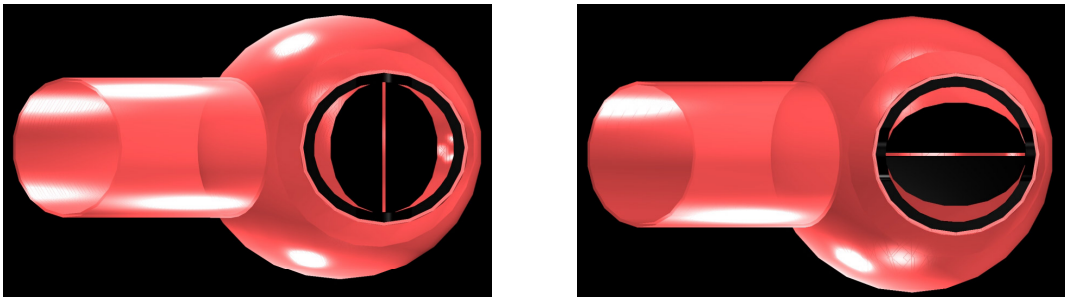

(a) (b)

Figure 2.3: (a) Anatomical and (b) anti-anatomical orientations studied in this effort.

2.3 St. Jude Medical Biocor Porcine Valve

The SJM Biocor porcine valve is manufactured from specially selected porcine triple-composite aortic valve cusps. In the present study, the SJM Biocor porcine heart valve was studied as a reference case considering that it is well known that biological valves such as this have a better hemodynamic performance as was discussed in the previous chapter, Section 1.2.1. Figure 2.4 shows the SJM Biocor porcine valve used in this study as was positioned in both the mitral and aortic positions.

Figure 2.4: St. Jude Medical Biocor porcine valve.

2.4 Pressure Transducers and Flow Rate Measuring Tools

To ensure the accuracy of the heart simulator, extensive pressure and flow rate measurements were obtained. A variety of sensors are available for the exploration of the behavior of the flow. Sensors traditionally employed in medical practice as well as instrumentation for fluid mechanics research have been employed so far.

The pressure transducer utilized was a catheter-based sensor by Millar Instruments and it allowed for measuring the absolute pressure, with atmospheric pressure being the reference. Furthermore, two ultrasonic flowprobes were also utilized and coupled with ultrasonic flow meters, model T110 by Transonic Systems, Inc. Both the pressure and flow rate sensors were employed in the setup of the present study and they were positioned upstream the mitral valve and downstream the aortic valve, hence before the entrance and after the exit flows of the left ventricular model.

2.5 DPIV

The ground of Particle Image Velocimetry was laid in the early eighties (reviews by Hasselinc (1989) and Adrian (1991) provide a detailed discussion) but it was the work of Willert and Gharib (1991), Westerweel (1993a, 1993b) and Huang and Gharib (1993) that established the digital implementation of PIV. Their work, as well as many other studies that followed, focus on a single-exposure, double-frame digital cross correlation approach. In addition, they focus on high-resolution (1Kx1K pixels) cameras that sample with up to 30 frames per second (fps), resulting in a sampling frequency of the flow field of only 15Hz. This is the major limitation of the DPIV systems that are commercially available. Yoganathan et al. (1998) describe the limitations of PIV for cardiovascular work and identify mainly the inability to distinguish between very high and very low velocities and the difficulty in recording pulsatile flow. These are serious limitations for the analysis of turbulent flows, where high frequency fluctuations are present. The system developed and used in this study overcomes all of these difficulties.

DPIV is based on the principle that the flow field of interest can be captured on video and consequently images of the flow field can be obtained to ultimately resolve the velocity field. Therefore, these images are a function of space and time and the temporal and spatial resolution of the method is dependent on the components and their integration. These components are a laser, special optics, and a camera. A two-dimensional slice of the flow field is illuminated by a light sheet, which is generated by the laser and passes through a special optical arrangement to form a

thin beam. Light is scattered in all directions by particles seeding the flow field. These particles must be able to accurately follow the flow field and there are specific parameters that must be accounted for when choosing the appropriate particle size. One such parameter is that the density of the particle should approximately equal the fluid density so to accurately respond to the flow fluctuations. The scattered light is detectable by the camera and images of the seeded flow field are captured successively with specified time intervals, which are typically very small, in the order of milliseconds or smaller. This time step has is dependent on the flow velocity and must be small enough to be able to capture the same groups of particles in successive images so that accurate particle tracking and displacement measurements of these particles will be able to resolve accurate velocity distributions. and an image similar to Figure 2.5(a) is obtained. A typical qualitative flow visualization image captured by the camera is shown in Figure 2.5 (a) prior to image processing and the corresponding processed quantitative image with velocity vectors is Figure 2.5 (b) below.

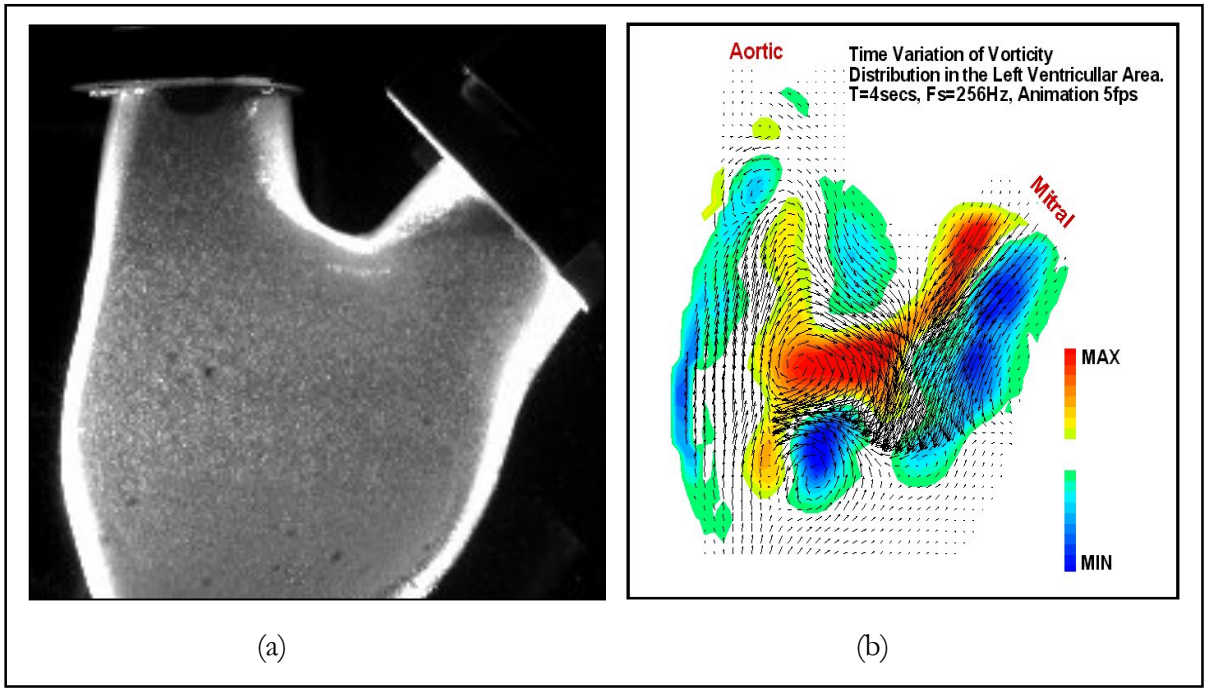

Figure 2.5: Qualitative flow visualization image prior to image processing (left) and corresponding quantitative PIV analysis result after processing (right).

2.5.1 Image Analysis and Processing

For image analysis, the image similar to Figure 2.5 (a) above is divided into small subdivisions or interrogation windows; usually square such as 32x32 pixels or 16x16 pixels. Each of these windows is processed independently to yield an individual displacement and therefore an independent velocity vector knowing the time step between the two images. The number of velocity vectors dependents on the size and number of the interrogation windows provided in the recorded image as well as the distance between the interrogation windows, which could be overlapped to generate a more populated velocity field.

In order to actually obtain a displacement for each interrogation window, a process called cross-correlation takes place. It is a mathematical operation that is generally implemented in the Fourier domain for reasons of computational efficiency. The best way to actually describe this process is to superimpose two successive images and allow translation vertically and horizontally to produce the highest pattern of particles in both images. Therefore, the corresponding displacement of the pattern of particles for the two images is the distance of separation between the two windows. In the present study, Visiflow, a commercially available package, allowed for analysis and application of the cross-correlation process of the qualitative flow visualization images resulting in instantaneous spatial maps of velocity fluctuations. Further analysis involved an in-house software which resulted in the vorticity and turbulent kinetic energy distributions for both steady and unsteady results which are presented in the following chapter.

2.5.2 DPIV Experimental Setup

DPIV can generate instantaneous velocity vectors along a plane that cuts the flow field. The current system uses a powerful 55-Watt pulsing laser that delivers a plane sheet of 2-mm thickness to illuminate the area of interest. The flow is seeded with neutrally buoyant fluorescent particles,

which serve as flow tracers. Particle diameters are in the order of 30 microns, in order to insure that the particles will accurately follow the flow with no response lag to any turbulent fluctuations. A very fast digital CMOS (Complementary Metal Oxide Semiconductor) imaging sensor, sampling at 1000 frames/sec and 512x256 pixel resolution, was integrated and employed to capture the instantaneous positions of the particles. The data are then processed, employing different software packages to return the instantaneous velocity fields. In the present experiment, a sampling frequency of 1000 Hz was used resulting to a total of 4000 time instants corresponding to 4 secs of data. The task of the velocity evaluation is carried using conventional cross-correlation between the particle image patterns of two consecutive frames. A total of 125x61 vectors with grid spacing of 600 microns and error in the order of +/- 0.005m/s are used to describe the flow field. The current DPIV system delivers sufficient temporal and spatial resolution to investigate the turbulent characteristics of the flow inside the LV. The authors are not aware of previous experiments that provide comparable spatio-temporal information for the character of the flow in the LV. During this experiment, one plane was interrogated cutting the span of the LV in the center as shown in Figure 2.6.

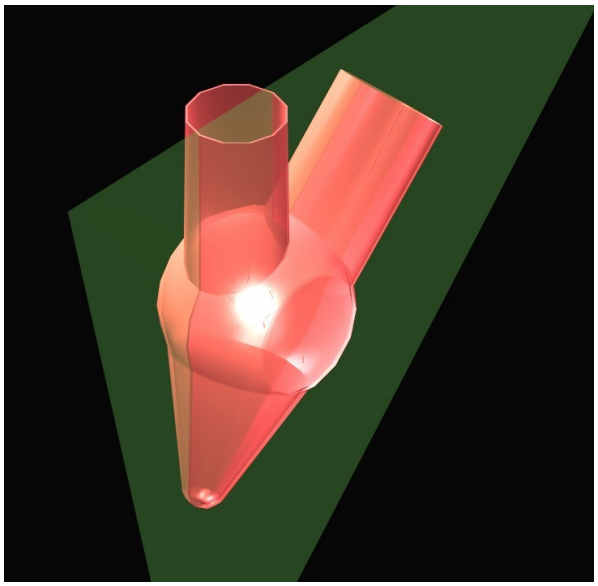

Figure 2.6: Location of the central plane along the span of the LV.

2.5.3 Hardware Component Details

The hardware components of DPIV were briefly mentioned in the above section, but specific details of each component are described in this section. The components are a copper vapor laser, a Phantom IV CMOS digital camera, D/A timer controllers, workstations, and optics.

The 55-Watt high frequency pulsing Copper Vapor laser has been the workhorse of DPIV as the left ventricle is the workhorse of the heart. The laser was developed in the ESM Fluid Mechanics Laboratory and has been used a large number of research projects. The nominal operational range of the laser is a 10 KHz frequency and power output pulse in the order of 5 mJ.

The Phantom IV camera by Vision Research Inc. delivers repetition rates up to 1000 frames per second (fps) for a 512x512 pixel resolution and up to 30,000 fps for a reduced image format. In the present study, as mentioned before, a resolution of 512x256 pixels at 1000 fps was utilized. The capabilities of this camera surpass those of conventional cameras used such a CCD (Charged Coupled Device) cameras, which are not as sensitive and have a lower signal to noise ratio.

Furthermore, two Digital/Analog Input Output boards were used during the project. The computer board's PCI-CTR05 timer counter board provided five independent counters with TTL signals and time resolution of 100 nsecs. High-end PC's were also used as workstations to provide the necessary computer processing capabilities. Also, a special combination of optics was used to obtain a beam thickness of 2-mm necessary for reducing the depth of field and distortion of out-of-plane particles.

Namely, the combination of the above components discussed increased the interrogation and spatial resolution by a factor of four, while our maximum time resolution has increased by one order of magnitude, which is approximately one thousand times the corresponding time resolution delivered by commercial DPIV systems. A typical arrangement of the experimental setup is illustrated in Figure 2.7.

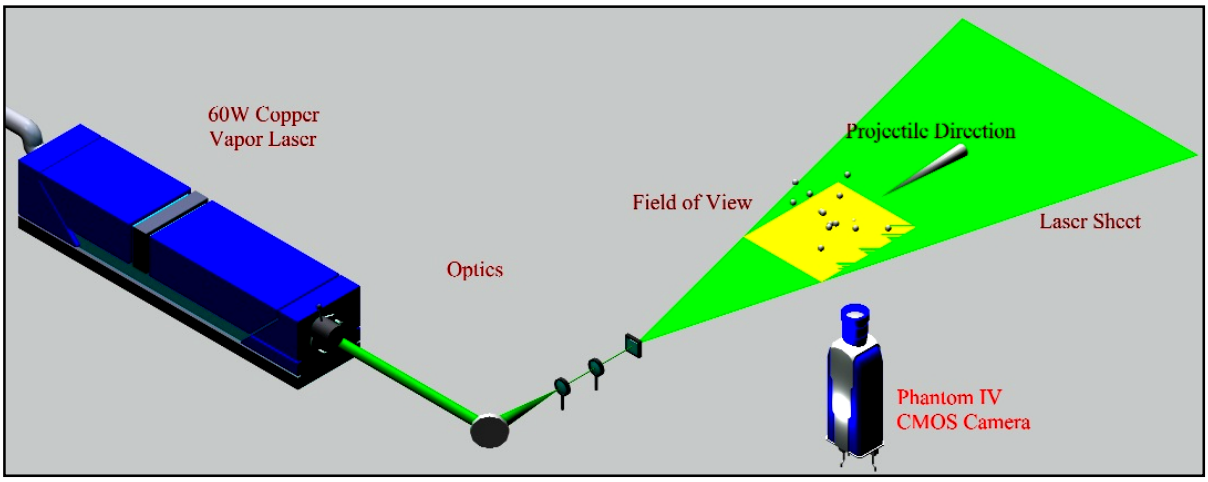

Figure 2.7: Schematic of experimental setup, which includes a 55-Watt Cu-Vapor pulsing laser, a high speed CMOS camera, optical lenses, and the flow field.

Chapter 3

3 EXPERIMENTAL RESULTS AND DISCUSSION

This chapter serves to illustrate DPIV results after image analysis and processing, which was discussed in the previous chapter. Both time-averaged and time-varying results are presented and compared among the three configurations. Initially, time-averaged results over 1100 instants obtained over a time interval of 1.1 seconds, or one heart cycle for the two mechanical orientations and the porcine valve are presented.

3.1 Pressure and Flow Rate Measurements

Extensive pressure and flow rate measurements were obtained to ensure the necessary testing parameters for running the heart simulator. Figures 3.1 and 3.2 show the flow rate curves in L/min taken during the experiment. The location of the two flow meter sensors was one upstream of the mitral valve and the second downstream of the aortic valve. From both figures, a periodic signal is observed as well as consistency in the shape of the signal among the three configurations, respectively the anatomical, anti-anatomical, and porcine cases.

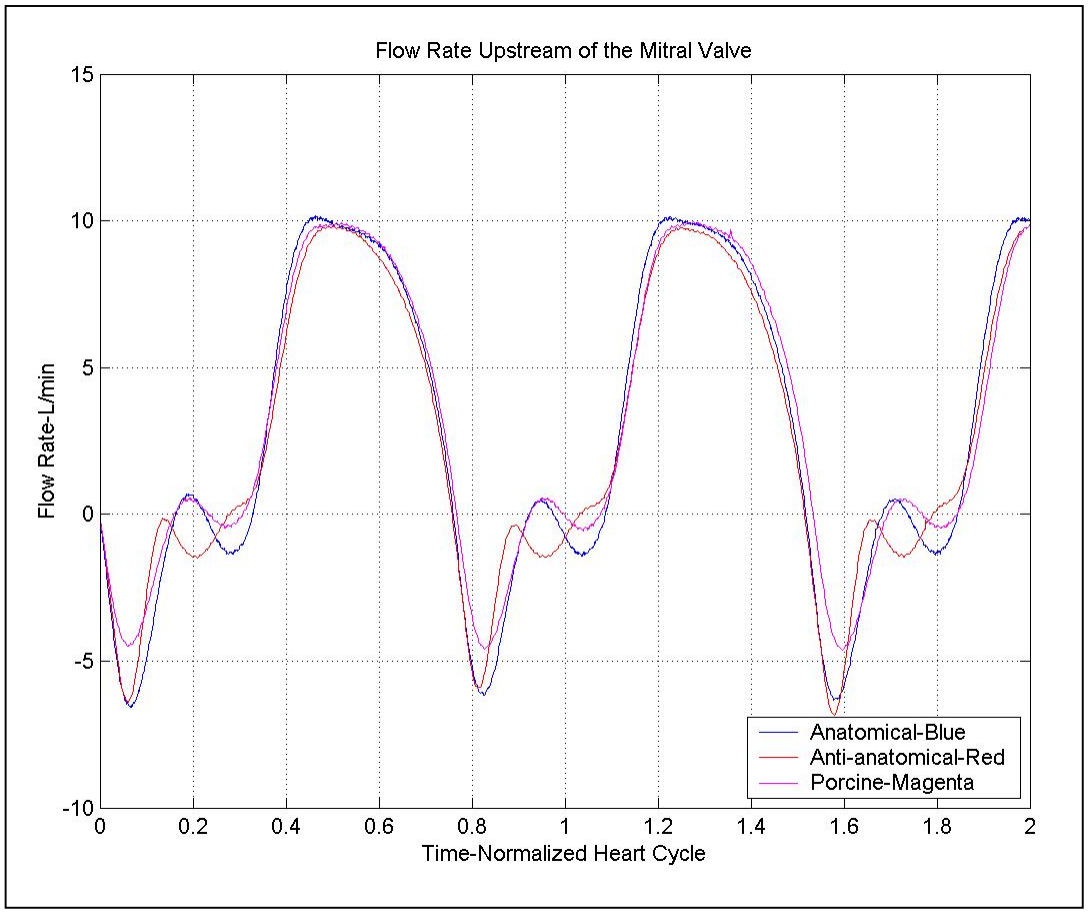

Figure 3.1: Flow rate measurements taken upstream of the mitral valve.

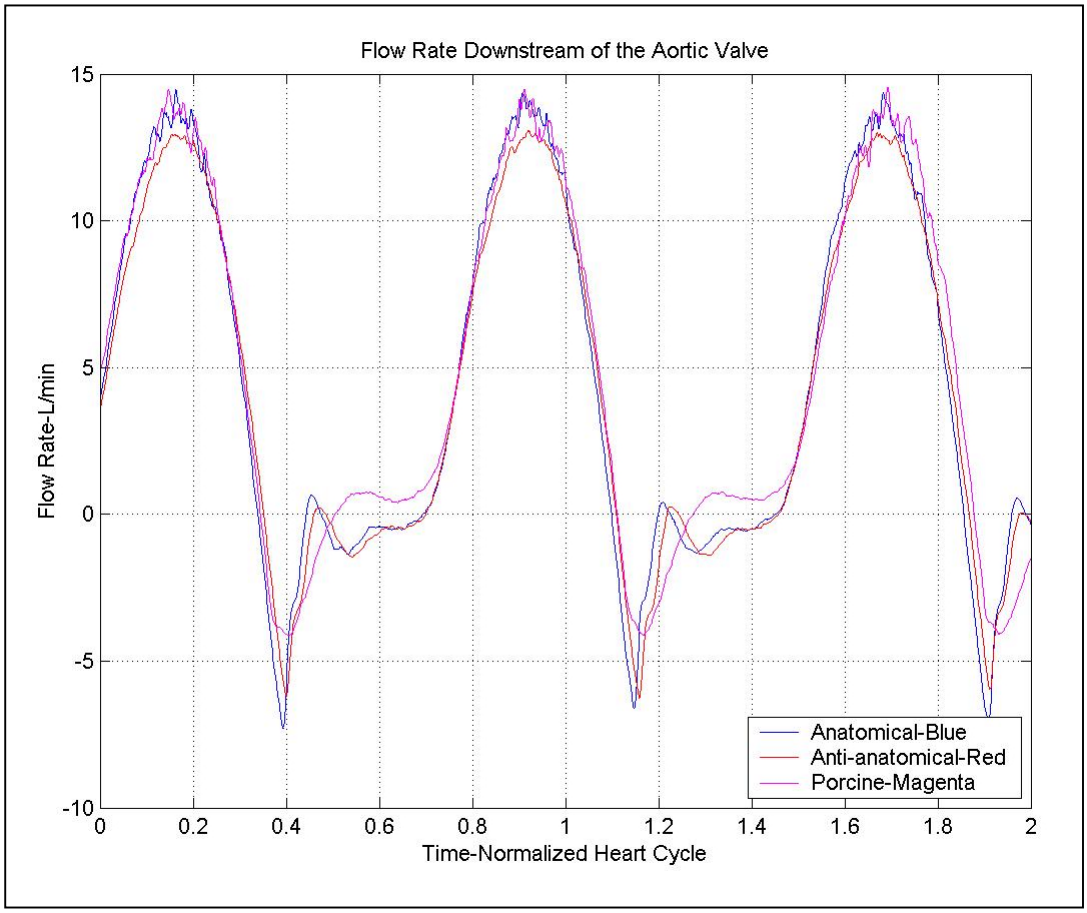

Figure 3.2: Flow rate measurements taken downstream of the aortic valve.

3.2 SJM Mechanical Mitral Valve Velocity Profiles

Figures 3.3 and 3.4 below represent a surface mapping of the velocity magnitude with respect to time and position along a line with 24 distinct points distal to the mitral valve for a total time of 2 secs for both cases. The peaks illustrate the mitral valve opening. As can be seen, there is big difference between the two orientations. Comparison of the two plots reveals a skewness that can be attributed to the time lag between the two leaflet openings as well as the asymmetry of the LV geometry. This phenomenon has also been observed in the past by other researchers.

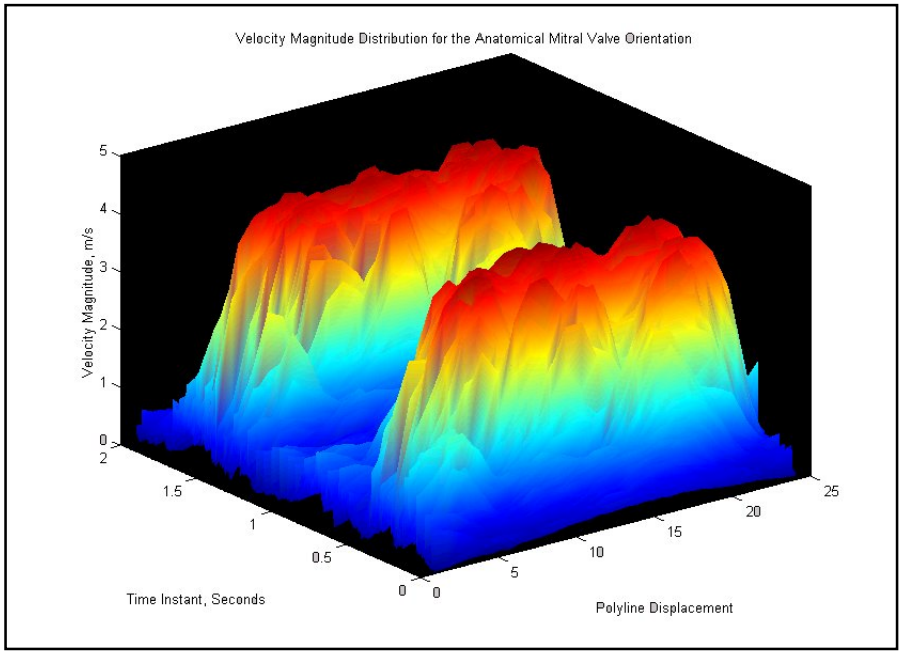

Figure 3.3: Instantaneous velocity profile downstream of the mitral valve for the anatomical valve orientation.

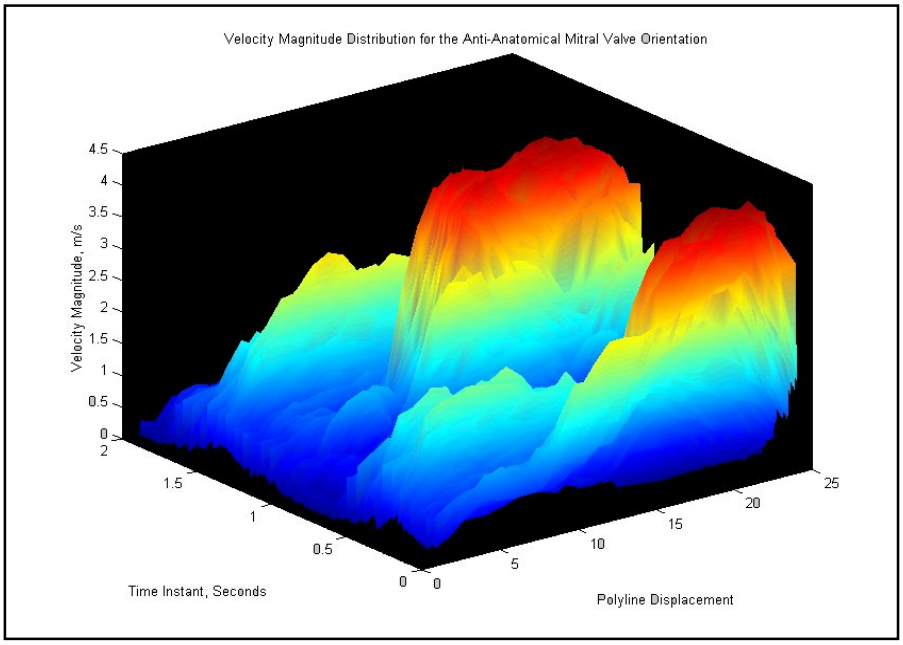

Figure 3.4: Instantaneous velocity profile downstream of the mitral valve for the anti-anatomical valve orientation.

With the above observation pertaining to the distinct velocity profile for each configuration, anatomical and anti-anatomical, it is believed that the LV filling would certainly be affected since the MV inlet jet differs.

Figure 3.5 below presents the instantaneous normalized hydrodynamic circulation defined by Equation 1,

$$\Gamma = \int_C \mathbf{V} \cdot d\mathbf{l} = \int_A \boldsymbol{\omega} \cdot d\mathbf{A} \qquad \text{(Equation 1)}$$

where Γ is circulation, $\mathbf{V}$ is the velocity vector, $\mathbf{l}$ is length, $\mathbf{A}$ is area, and $\boldsymbol{\omega}$ is vorticity. Instantaneous values of circulation are calculated by integrating vorticity over the rectangular region in the center of the left ventricle as shown in the bottom right corner of Fig. 3.5. The results correspond to the net circulation within the area over one heart cycle as resulted by averaging both

positive (counter-clockwise vorticity) and negative (clockwise vorticity) values. Physically, circulation represents vortex intensity. Although the averaging over a certain areas acts as a spatially low pass filter, highly unsteady fluctuations can be deduced from Figure 3.5. Highly unsteady turbulent fluctuations can be deduced from this figure. For the anatomical orientation, the changes in sign can be attributed to the vortex shedding from the mitral leaflets. Higher fluctuations, which correspond to turbulence, are present in the case of the anatomical orientation. When compared to those of the anti-anatomical case, these fluctuations are damped and a more coherent flow field is generated.

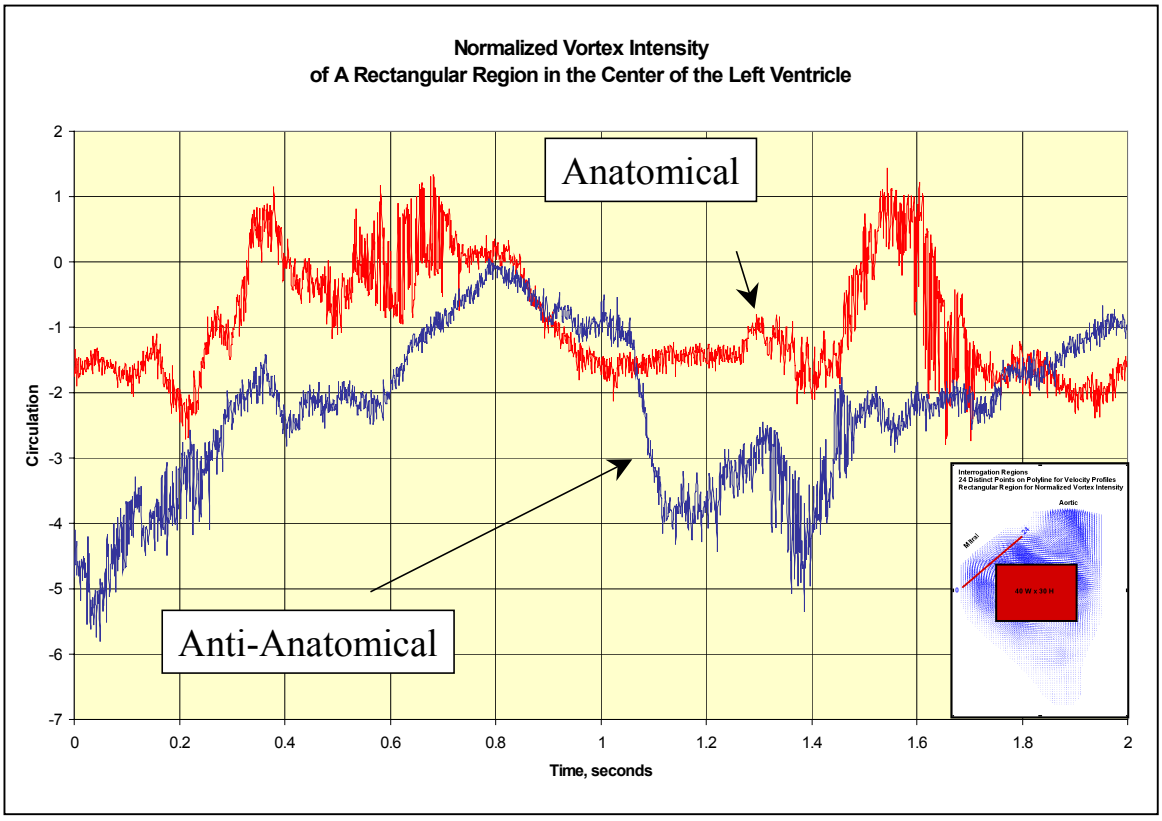

Figure 3.5: Normalized vortex intensity for all configurations of rectangular region in the center of the left ventricle.

3.3 Vorticity Distributions

Both time-averaged and time-varying results are presented and compared for the three configurations. Namely, the two orientations of the SJM MHV, anatomical and anti-anatomical, and the porcine valve were studied. Contours of the vorticity component normal to the plane of interrogation as well as streamline, velocity, and turbulent kinetic energy distributions are presented in the following sections. Clockwise vortical motion is denoted by negative vorticity, which is presented in terms of blue color contours. Counter-clockwise vorticity is presented in terms of shades of red.

Time-averaged results over 1100 instants obtained over a time interval of 1.1 seconds, or one heart cycle for the three cases are presented for each case respectively in Figures 3.6, 3.7, and 3.8. Although time-averaged results conceal the unsteady and pulsatile character of the flow, they do provide valuable information. By averaging within one period of the heart cycle, we can reveal the prevailing flow structures that persist in the flow for an extended duration within the period, while the randomness of the flow averages to small values very close to zero.

Significant differences are observed by comparing the character of the flow between the three different configurations. In a time-averaged sense, for all three cases, Figures 3.6, 3.7, and 3.8, we observe the presence of two well-organized counter-rotating vortices in the immediate vicinity of the aortic valve (AV). This indicates that these structures survive throughout the duration of a heartbeat, which illustrates the presence of vortical structures that do not diffuse and induce a low-pressure region, which in turn enhances regurgitation and reduce the efficiency of the LV. Specifically, in the case of the anatomical orientation, Figure 3.6, this vortex pair upstream of the AV appears to be stronger encompassing a larger region than in the other two cases. Moreover, from Figure 3.6, when the mitral valve (MV) is in the anatomical orientation, six distinct high vorticity regions are revealed and are attributed to the interaction of the three entrainment jets. However, in Figure 3.7, corresponding to the anti-anatomical orientation, three distinct jets are not apparent but rather the formation of a very strong negative (clockwise) vortex dominating the

center area is observed. Similarly, Figure 3.8, showing vorticity distributions of the porcine valve, reveals in a time-averaged sense a large region of negative vorticity but with less intensity than in the two orientations of the SJM bileaflet MHV.

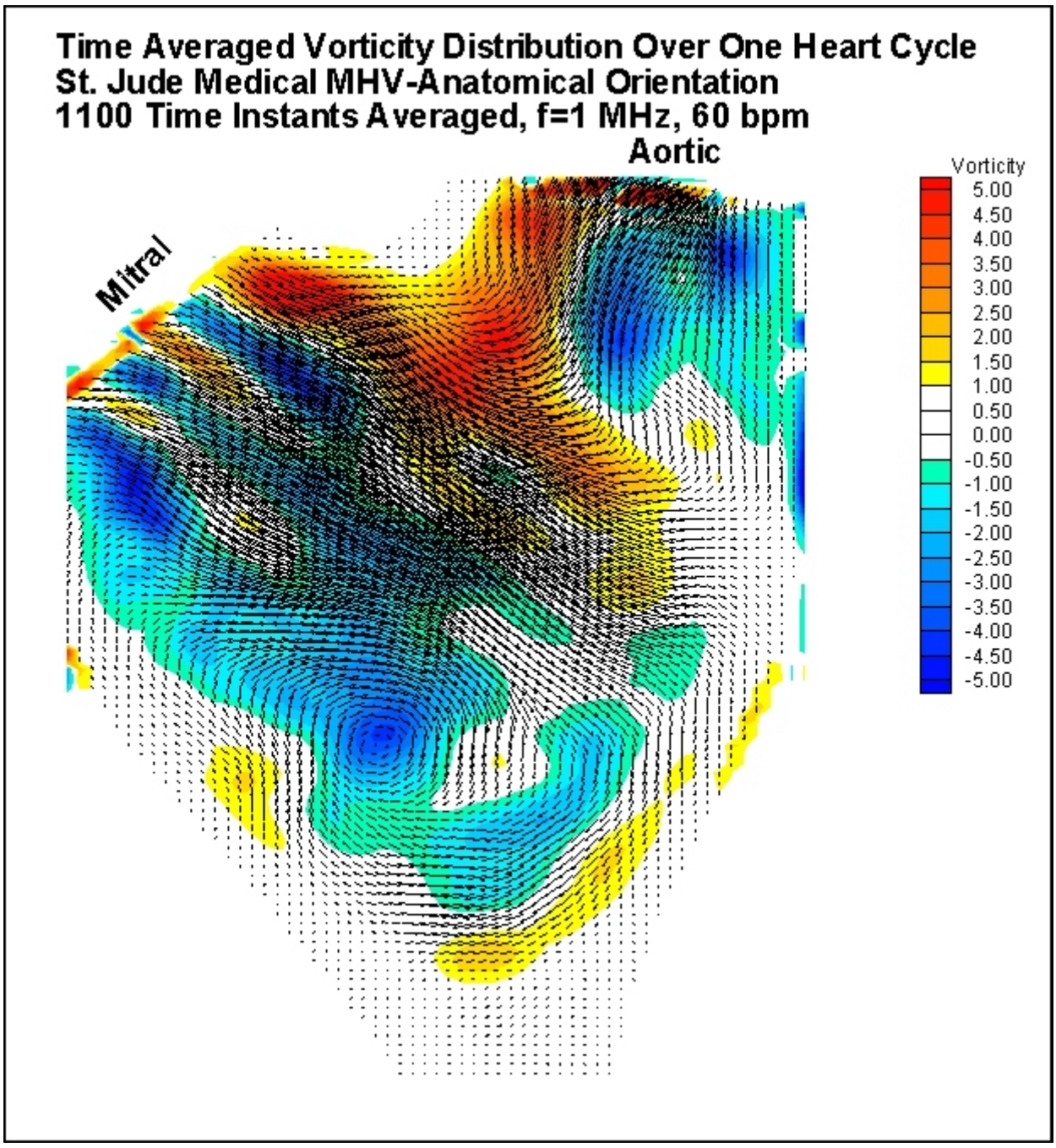

Figure 3.6: Time averaged vorticity and velocity distributions over one heart cycle for the anatomical orientation.

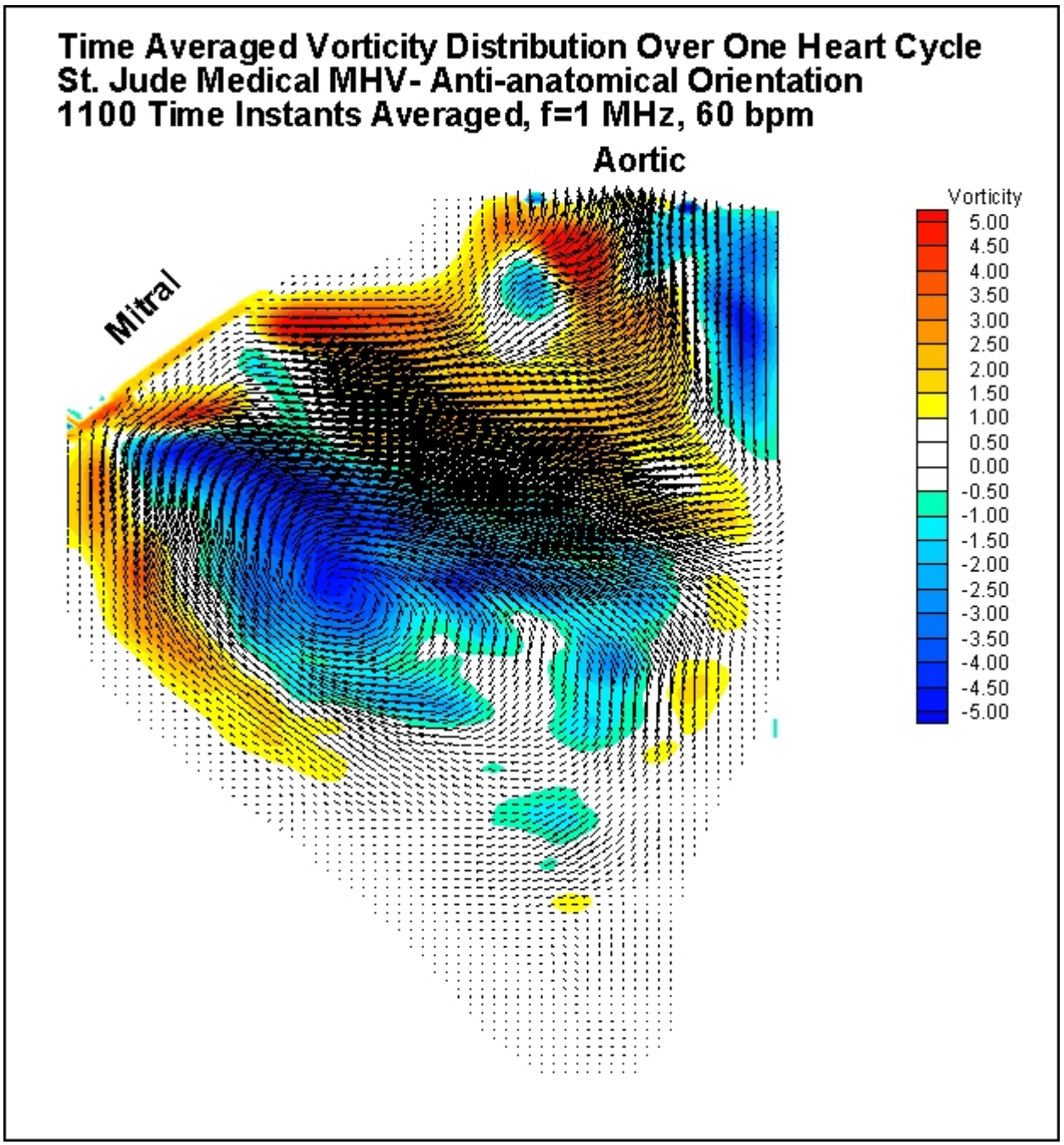

Figure 3.7: Time averaged vorticity and velocity distributions over one heart cycle for the anti-anatomical orientation.

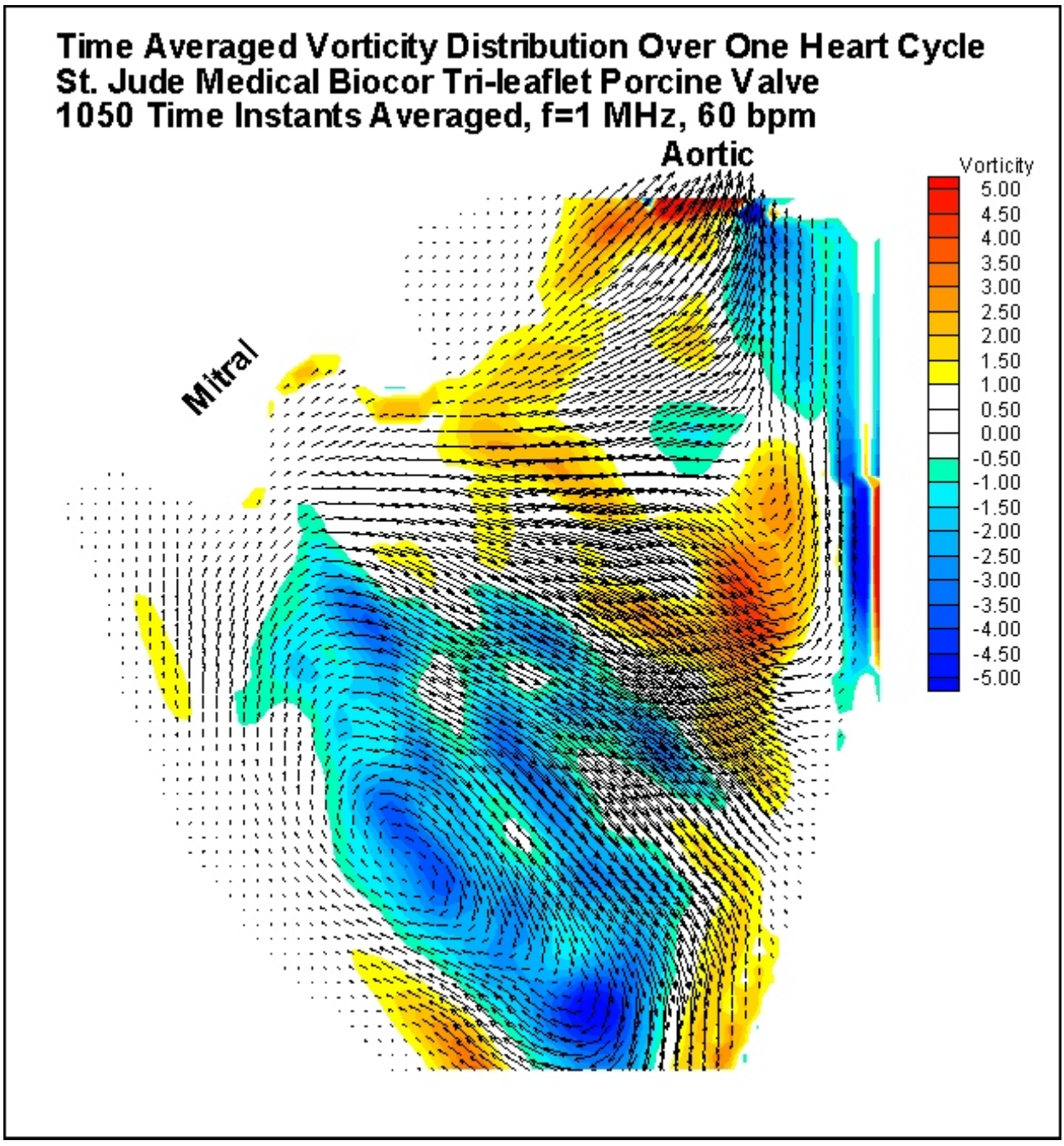

Figure 3.8: Time averaged vorticity and velocity distributions over one heart cycle for the porcine configuration.

From these figures, two mechanisms that could potentially compromise the performance of the LV are identified. The first mechanism is associated with the presence of a vortical structure in a time-average sense near the aortic valve, which indicates a coherent vortex that does not diffuse within the cycle. The underlying physics reveal that the asymmetry of the incoming jet through the mitral valve encourages the propagation of the vortex towards the AV with an induced vortex velocity downward. In turn, when the aortic valve is closed and a vortex is present upstream of the valve, there is an increase in the transvalvular pressure that enhances regurgitation. As a result, a low-pressure region proximal to the aortic valve increases the transvalvular pressure gradient. This effect could contribute to enhancing regurgitation and reducing the efficiency of the LV. The second mechanism is related to the energy loss through the formation of vortical structures in the LV. In the anatomical orientation, high levels of vorticity and velocity fluctuations are present and are attributed to the three strong inlet jets. In contrast, the anti-anatomical orientation illustrates a smoother velocity distribution as well as a more coherent vortical structure in the central region.

Figure 3.9 is a plot of instantaneous normalized circulation over one heart cycle for all three cases in a rectangular region upstream of the AV. Considering the fact that pressure difference is proportional to the square of circulation of the vortex, it can be deduced that the anatomical case would yield a higher level of regurgitation. The porcine case would in turn generate the least amount of regurgitation.

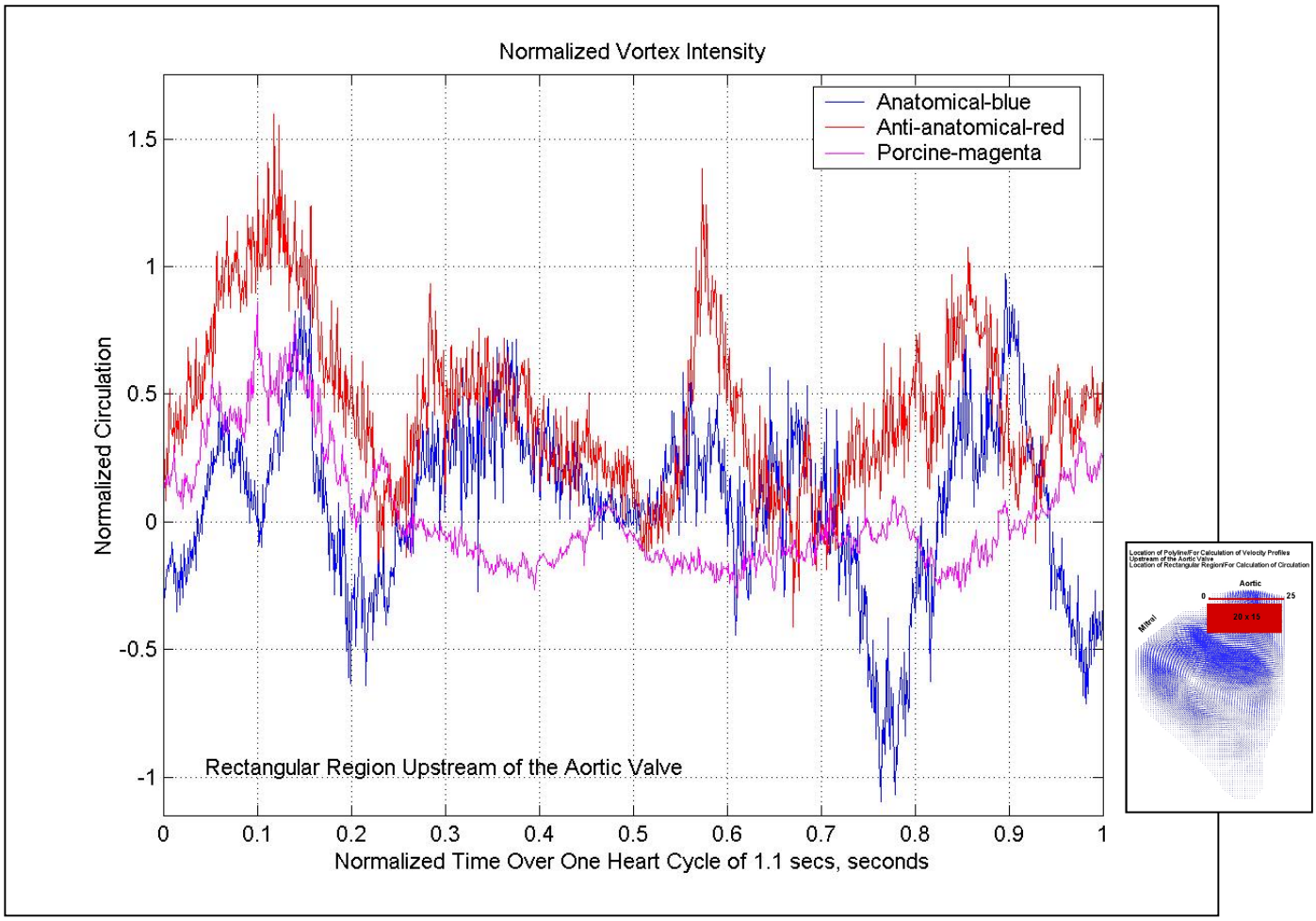

Figure 3.9: Plot of normalized circulation over one heart cycle in a rectangular region upstream of the aortic valve for the three cases of anatomical, anti-anatomical, and porcine orientations.

Significant differences are observed by comparing the character of the flow between the three different configurations in Figure 3.9. For the first case, corresponding to the anatomical orientation, we observe that the interaction of the three entrainment jets generate high vorticity in the vicinity of the MHV leaflets. Two counter rotating vortices are also present in the region near the aortic valve (AV). On the contrary, the anti-anatomical orientation results in the formation of a

very strong coherent vortex that dominates the center area of the LV. This significant difference in the flow structures present in the LV can be attributed to the fact that in the anatomical orientation, the interaction of the shear layers shed from the leaflets generate small-scale eddies that result into a more turbulent flow field while for the anti-anatomical orientation the flow structures are more organized.

3.4 Turbulent Kinetic Energy Distributions

Figures 3.10, 3.11, and 3.12, corresponding to the three configurations, confirm the aforementioned observation, pertaining to both the inlet MV jet vorticity levels and the presence of two counter rotating vortices upstream of the AV, as it presents the time averaged planar turbulent kinetic energy. The anatomical orientation, Figure 3.10, shows extended regions of high turbulence distal to the MV, while the corresponding turbulence levels for the anti-anatomical orientation, Figure 3.11, are confined in a smaller area. In addition, high turbulence levels are also present upstream of the AV for both orientations of the bileaflet MHV. In contrast, the case of the porcine configuration, Figure 3.12, contains lower turbulence levels when compared to the flow through MHVs illustrating a more structured flow. The vorticity and turbulent kinetic energy are concentrated in the center in the porcine case. Previous clinical studies have shown the porcine valve to offer better hemodynamic performance than MHVs. The present results serve to quantity this observation by illustrating the complex spatio-temporal development of flow structures and turbulence inside the LV.

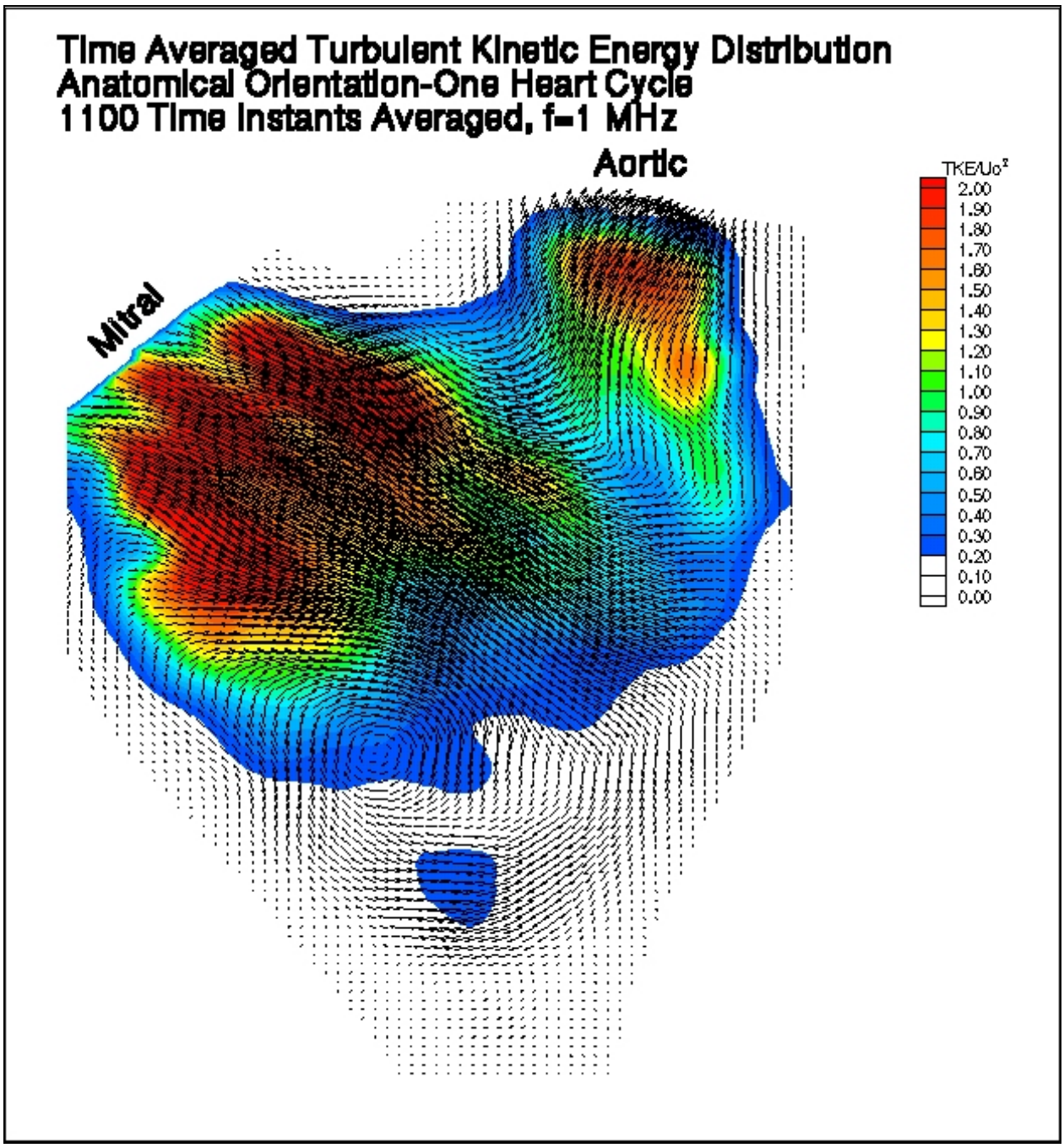

Figure 3.10: Time averaged turbulent kinetic energy over one heart cycle for the anatomical orientation.

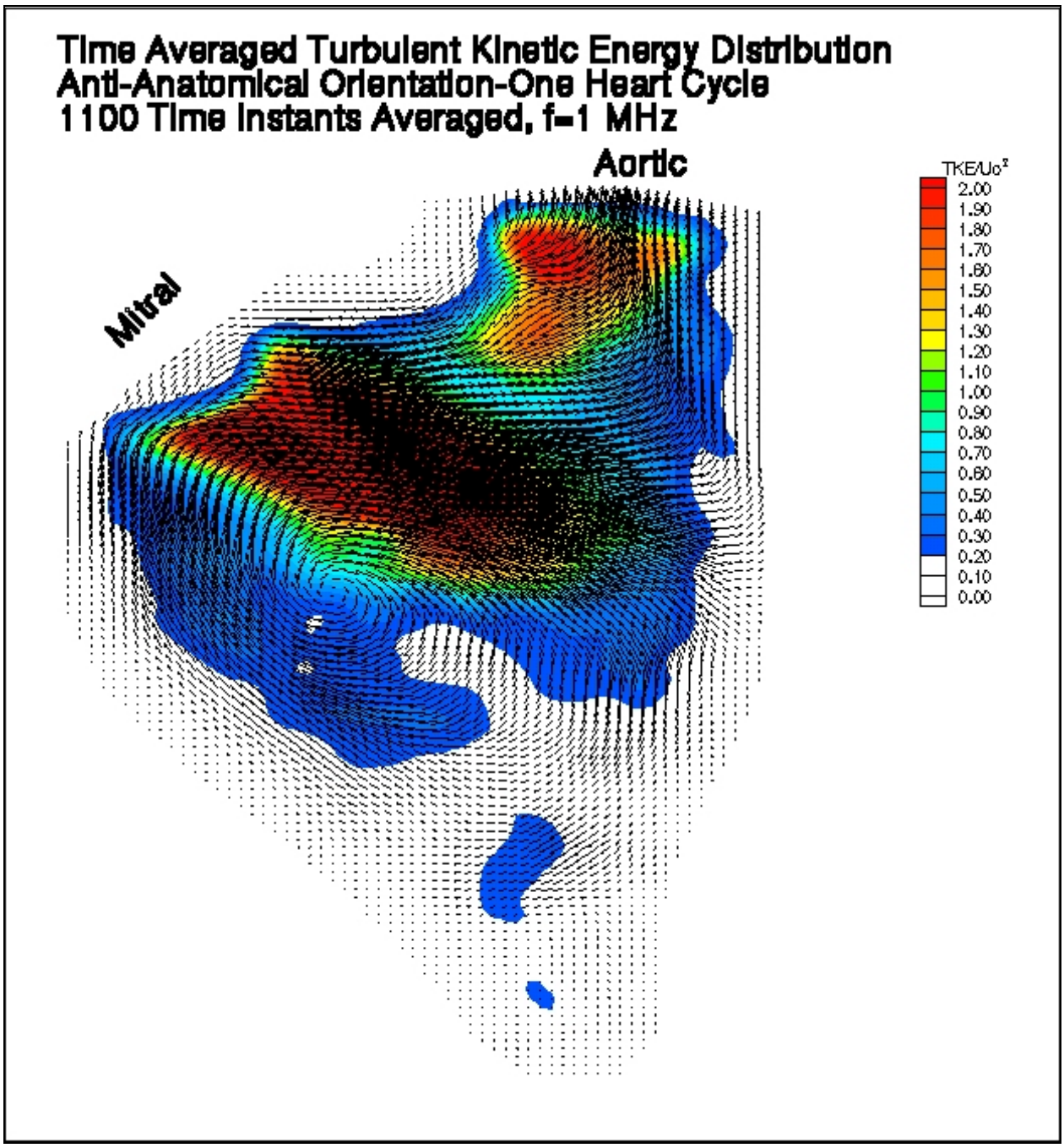

Figure 3.11: Time averaged turbulent kinetic energy over one heart cycle for the anti-anatomical orientation.

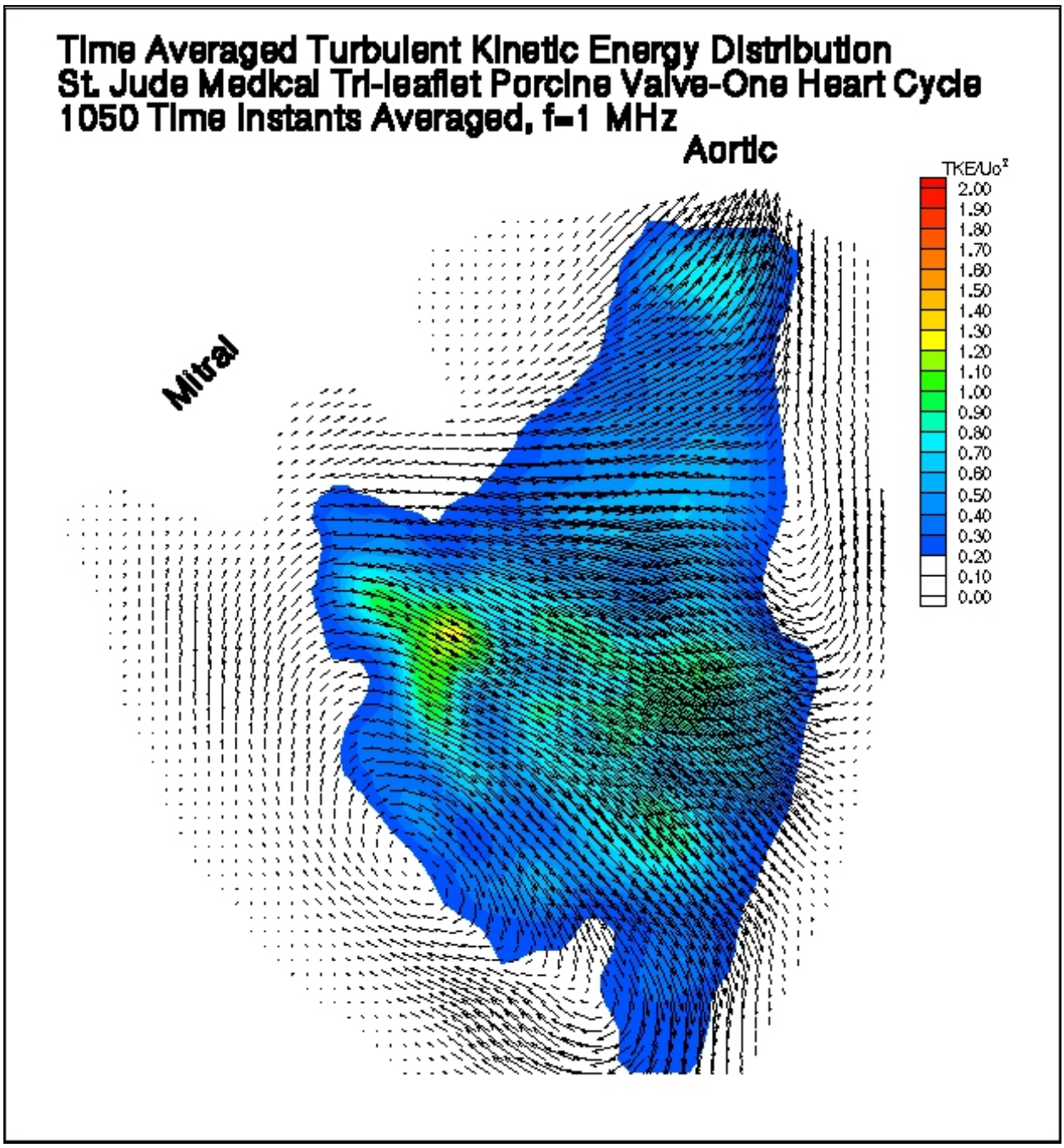

Figure 3.12: Time averaged turbulent kinetic energy over one heart cycle for the porcine configuration.

Moreover on the issue involving high turbulence levels present upstream of the AV, the following conclusions can be made. Considering the fact that the region proximal the AV is dominated by the high-speed flow that exits the LV, high intensity turbulence can be attributed to the large-scale vortex that forms during the diastolic part of the cycle and subsequently gets convected through the aortic valve during the systolic part. For the porcine configuration, it is evident that the flow is more structured with lower vorticity and turbulence levels when compared to the mechanical orientations.

The time-averaged turbulent kinetic energy distributions provide a qualitative measure of the efficiency of the LV. The high levels of turbulent kinetic energy quantify the energy content of the vortical structures present in the LV. Once the energy contained in the entrance jets of the mitral valve roll into three-dimensional vortices, this energy is lost and there are no physical means to recover it. Thus, comparing the three configurations provides evidence that the turbulent losses are significantly enhanced in the anatomical case.

3.5 Time Varying Vorticity Distributions

Similar conclusions can be derived from the time varying results. However, a complete assessment of the unsteady information can be achieved only by animating the entire time sequence. For that reason, animations, corresponding to the anatomical, anti-anatomical, and porcine configurations respectively, of instantaneous velocity and vorticity distributions over one complete heart cycle are accompanied as AVI files with the thesis. In view of the fact that it is difficult to discuss in detail the entire animated sequence of 1100 time instants, four specific time instants within the heart cycle have been chosen. The corresponding time instants that will be discussed in more detail are T= 0 secs, T = 0.33 secs, T = 0.43 secs, and T = 0.63 secs. Once again, clockwise vortical action is denoted by negative vorticity, which is presented in terms of red color contours. Counter-clockwise vorticity is presented in terms of shades of blue.

Figures 3.13, 3.14, and 3.15, corresponding to T = 0 secs for the three configurations, represent the initiation of the heart cycle when the mitral valve is fully open and strong vortical structures distal to the MV are generated. In the case of the anatomical orientation, Figure 3.13, the leaflets form six regions of high shear flow. These correspond to the three inlet jets, which contain the highest levels of vorticity and encompassing a larger region when compared to the anti-anatomical and porcine configurations. The MV incoming jet in the case of the anti-anatomical orientation, Figure 3.14, reveals a more coherent and less dispersed entrance jet. Additionally, Figure 3.15, corresponding to the porcine configuration, reveals an even more dispersed MV inlet jet and the high variation of vorticity is due to the flattering of the leaflets. Furthermore, when looking at the two orientations of the mechanical heart valve (MHV), high vorticity is present upstream of the AV and is associated to the two counter-rotating vortices. This was also observed in the time-averaged velocity and vorticity distributions, which were discussed above, and serves to illustrate that these vortical structure survive the diastolic phase, as they do not diffuse. Also, considering that these vortical structures are a low-pressure region, their presence could potentially increase the transvalvular pressure across the AV and result in enhancing regurgitation. It is important to note that this is not observed in the porcine case, as would be expected. Lastly, during this time instant, another distinct difference between the two orientations of the MHV and the porcine case pertains to the region near the apex. In this region, stagnant flow is observed for the anatomical and anti-anatomical orientations but not in the porcine case. Stagnant flow has the implication of slow moving and recirculating flow that could result in thrombus formation and clotting.

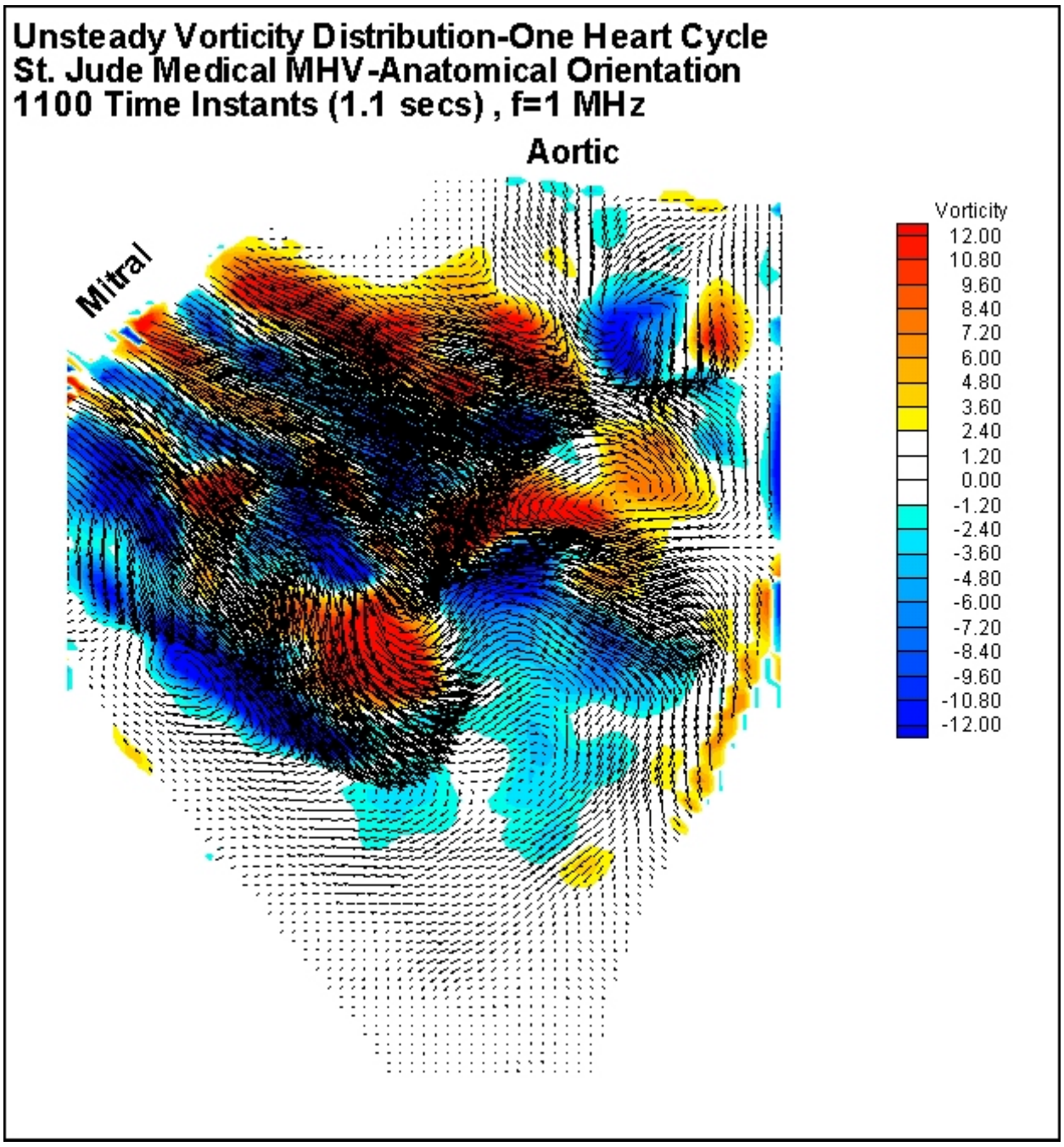

Figure 3.13: Time-varying vorticity and velocity distributions for T = 0 secs for the anatomical orientation.

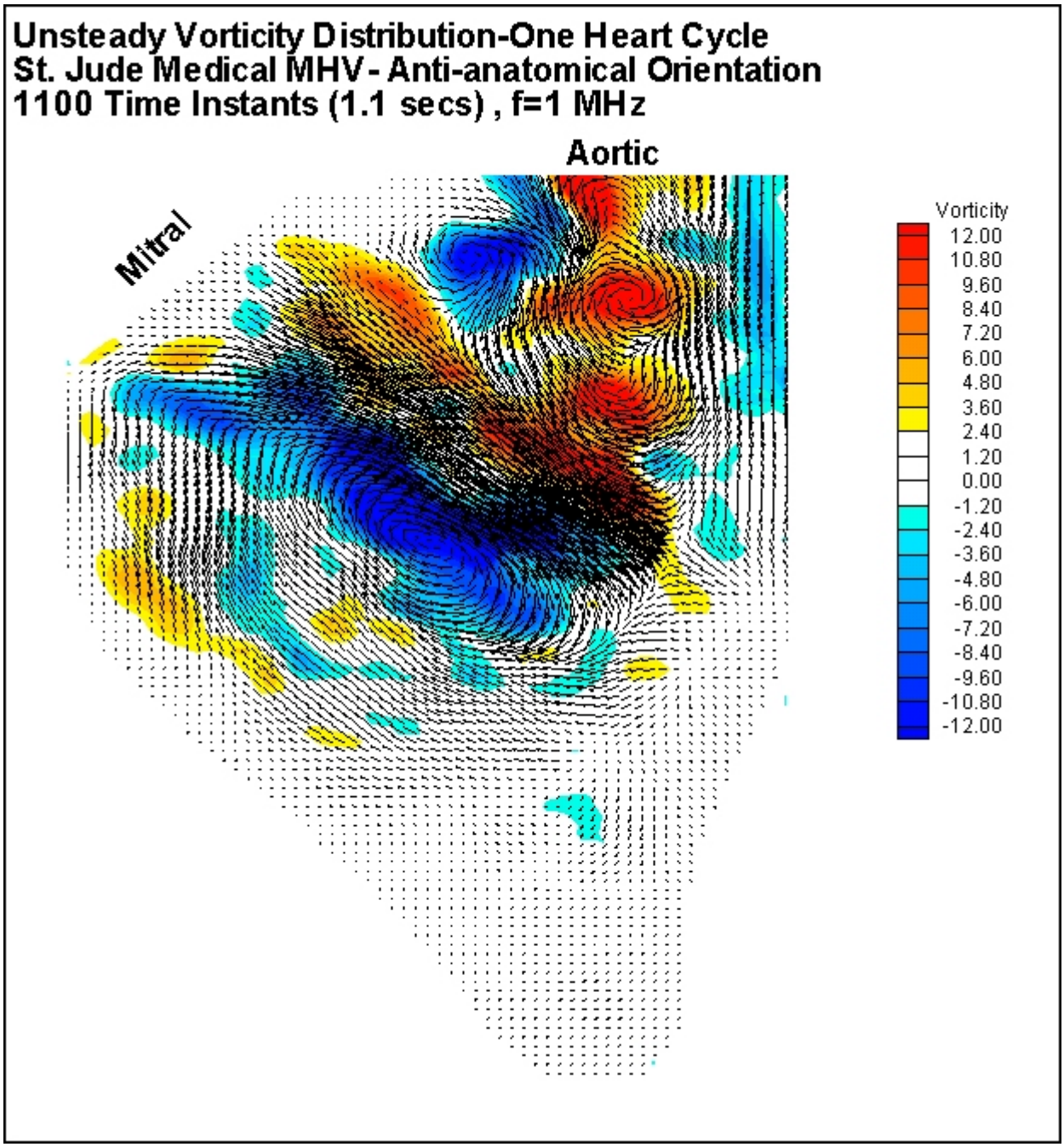

Figure 3.14: Time-varying vorticity and velocity distributions for T = 0 secs for the anti-anatomical orientation.

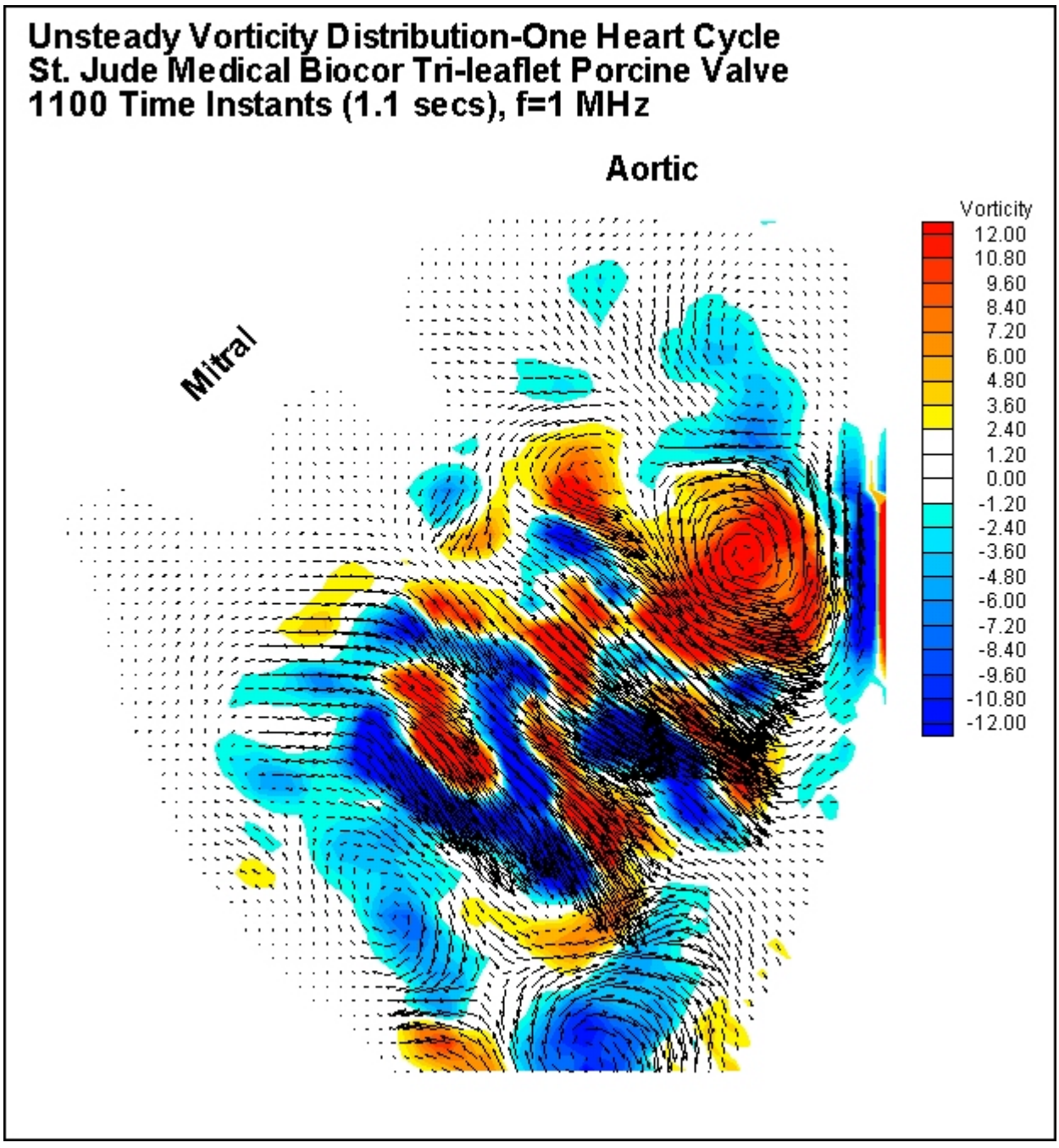

Figure 3.15: Time-varying vorticity and velocity distributions for T = 0 secs for the porcine configuration.

The second time instant of T = 0.33 secs, Figures 3.16, 3.17, and 3.18, illustrates the mitral valve fully closed and the initiation of the aortic valve opening. High vorticity and a strong exit jet in the region of the aortic valve are present. Figures 3.16 and 3.17, corresponding to the anatomical and anti-anatomical orientations respectively, illustrate MV regurgitation, which is not observed in the porcine case, Figure 3.18. Furthermore, two large-scale counter-rotating vortices are present in the LV for the two orientations of the MHV. Kinetic energy is trapped within these vortical structures and it cannot be recovered. This would compromise the efficiency of the heart. Figure 3.18, porcine configuration at T = 0.33 secs, reveals a different flow structure. Specifically, only one large-scale clockwise vortex is present in the center and it helps redirect flow outward. It is also important to note that at this time instant the interaction of the primary vortex with the walls results in the generation of secondary vortices. These vortices interact with the primary vortex but the time needed for this structures to lose their coherence appears to be larger than one heartbeat.

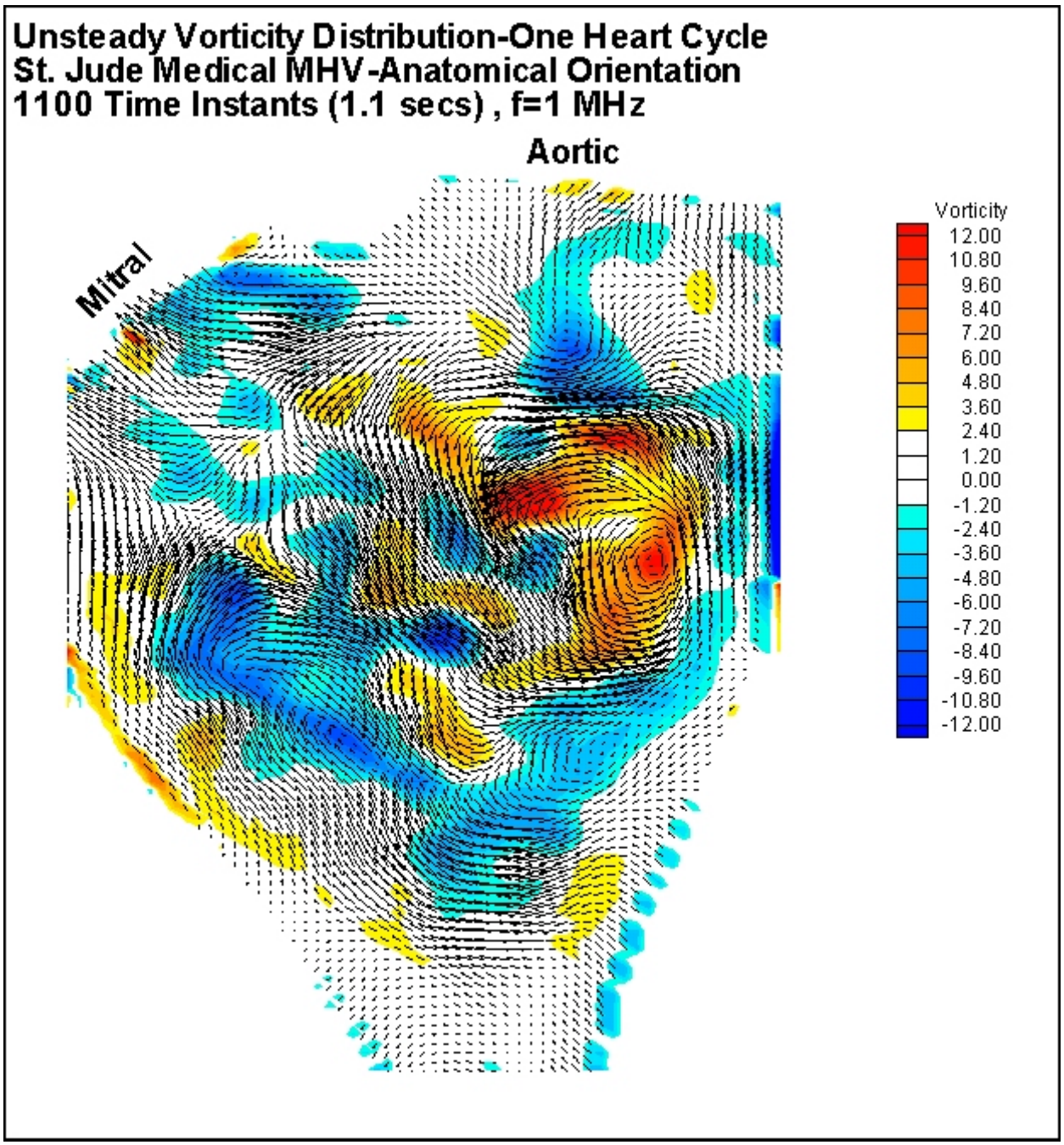

Figure 3.16: Time-varying vorticity and velocity distributions for T = 0.33 secs for the anatomical orientation.

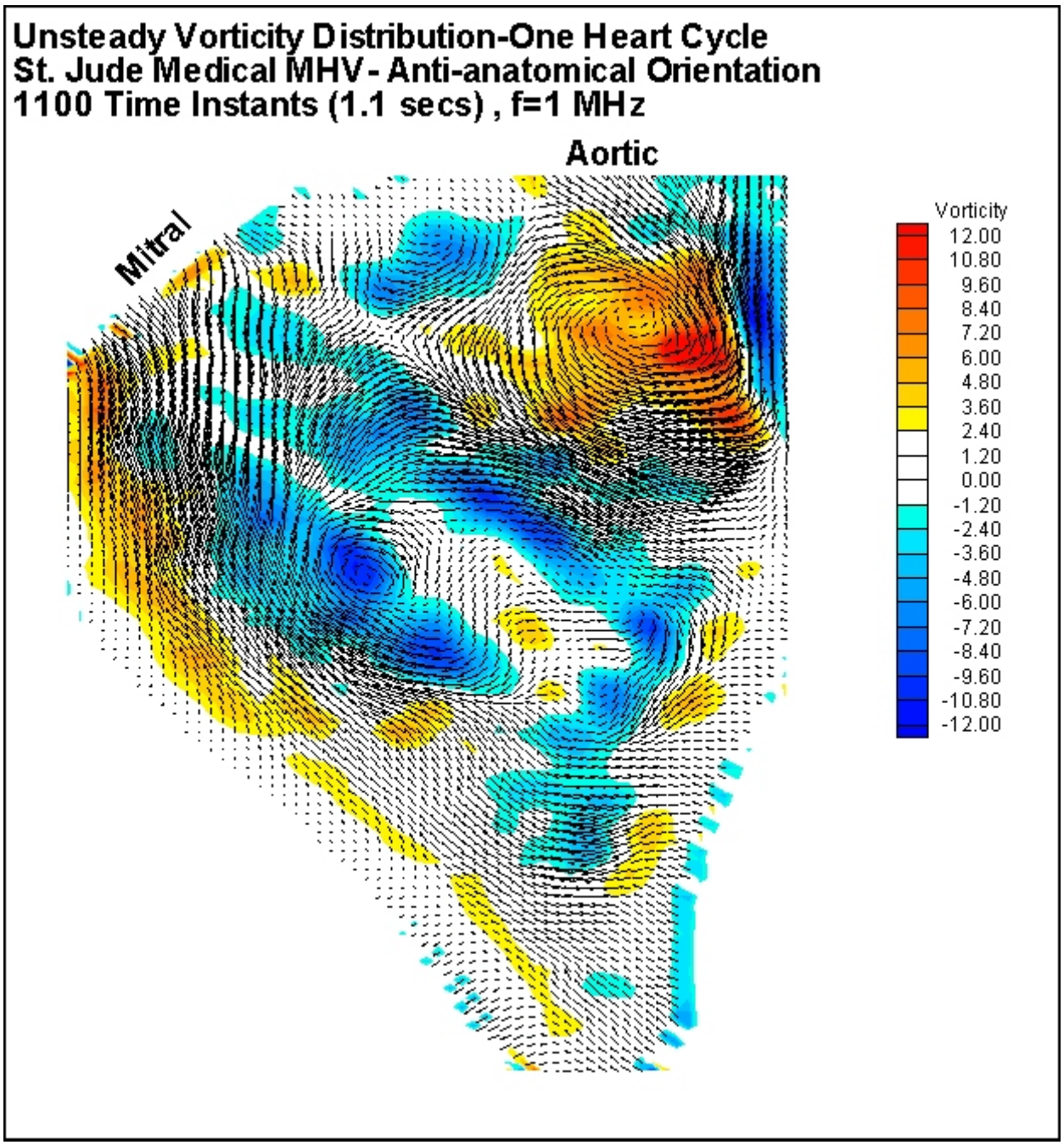

Figure 3.17: Time-varying vorticity and velocity distributions for T = 0.33 secs for the anti-anatomical orientation.

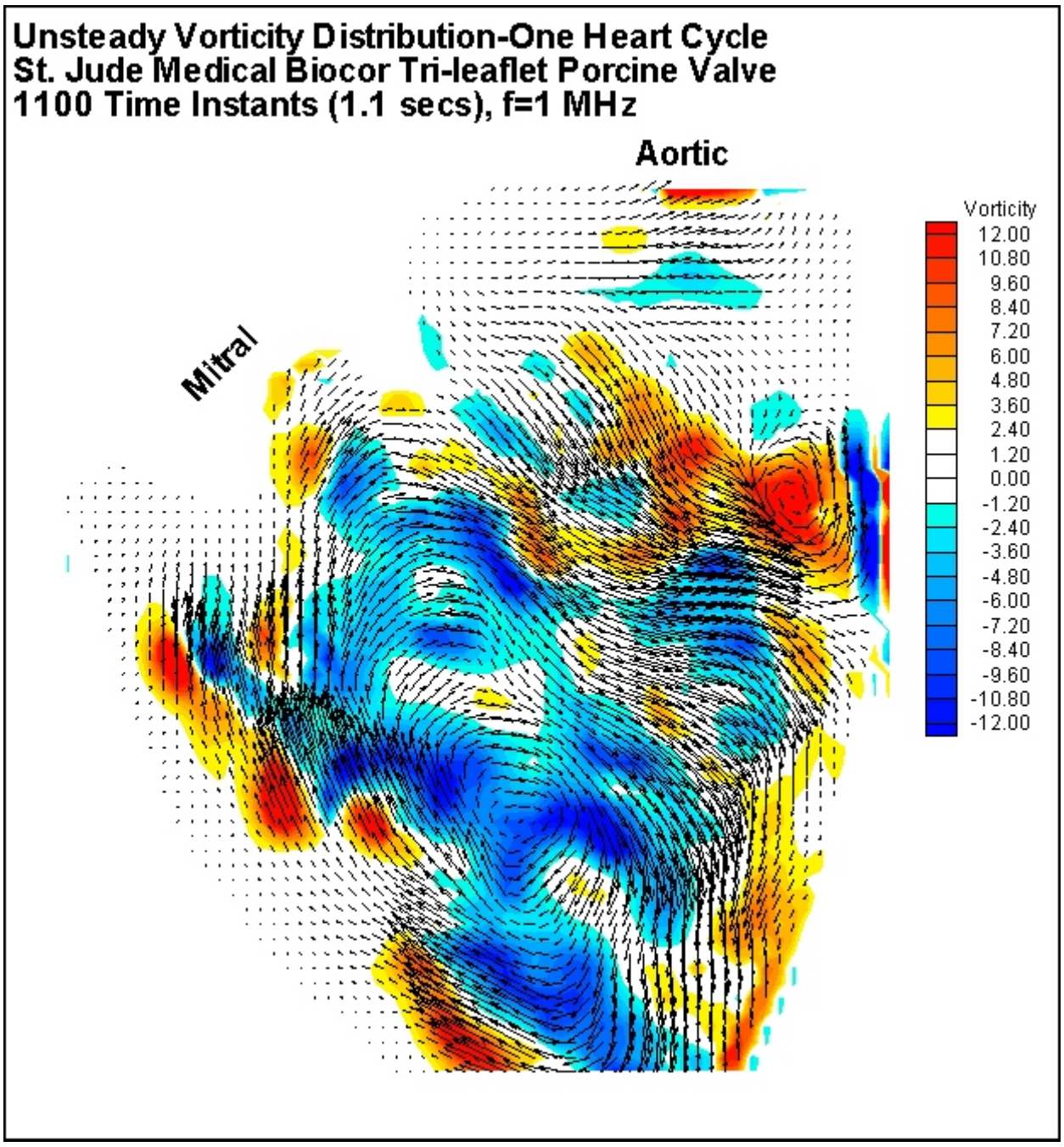

Figure 3.18: Time-varying vorticity and velocity distributions for T = 0.33 secs for the porcine configuration.

By the time that the aortic valve is fully open at time T = 0.43 secs, Figures 3.19, 3.20, and 3.21, the vortical structures discussed in the previous time instant are still coherent and strong as they get pushed out of the LV. They survive the diastolic cycle. More specifically, in the case of the anatomical orientation, Figure 3.19, a large-scale vortex is present in the center of the LV but appears to be physically lower than the vortex present in the anti-anatomical orientation, Figure 3.20. Furthermore, the vortical structure in the anatomical case is stronger and encompasses a larger region when compared to the anti-anatomical configuration. The porcine case is more similar to the anti-anatomical configuration.

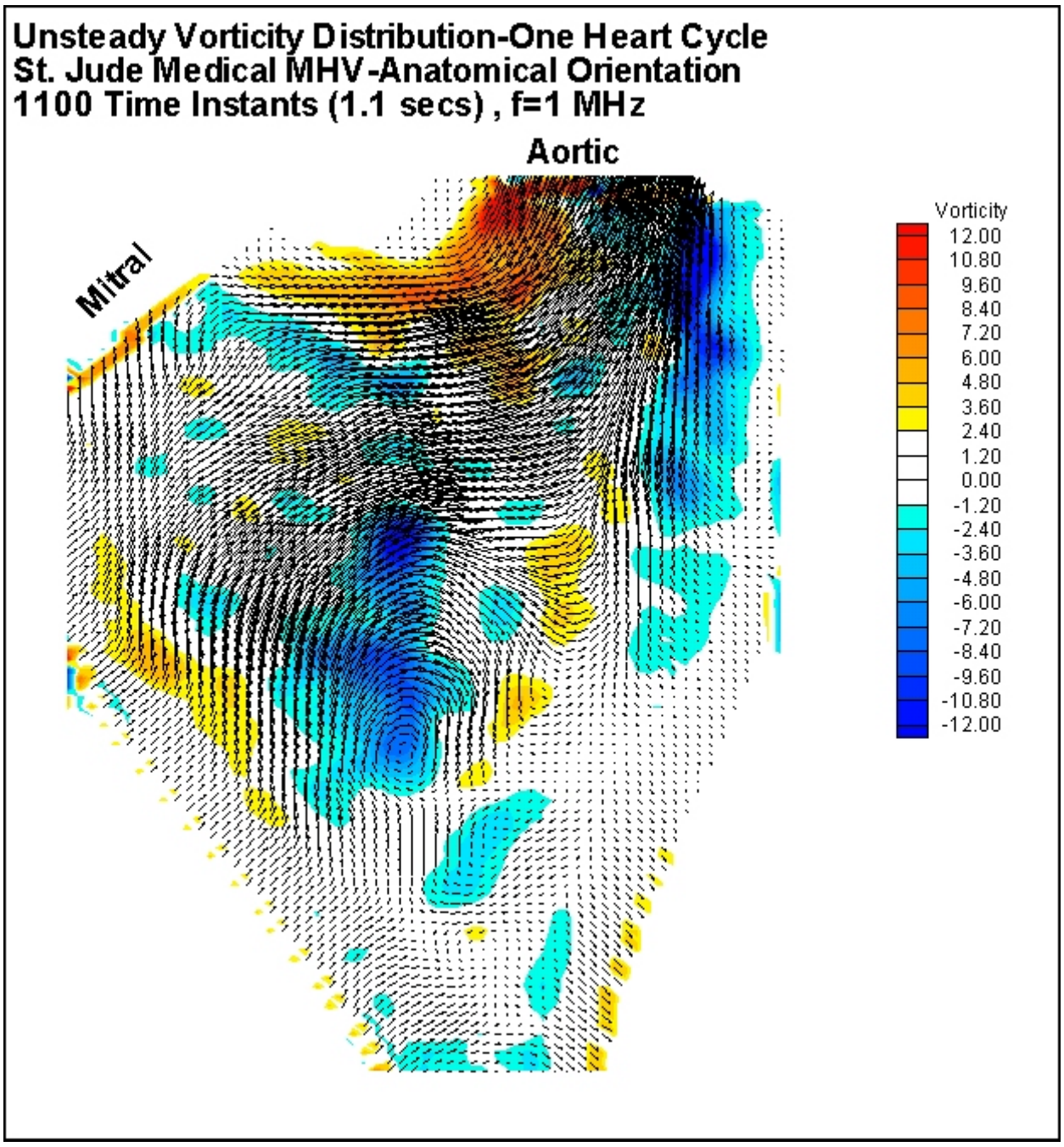

Figure 3.19: Time-varying vorticity and velocity distributions for T = 0.43 secs for the anatomical orientation.

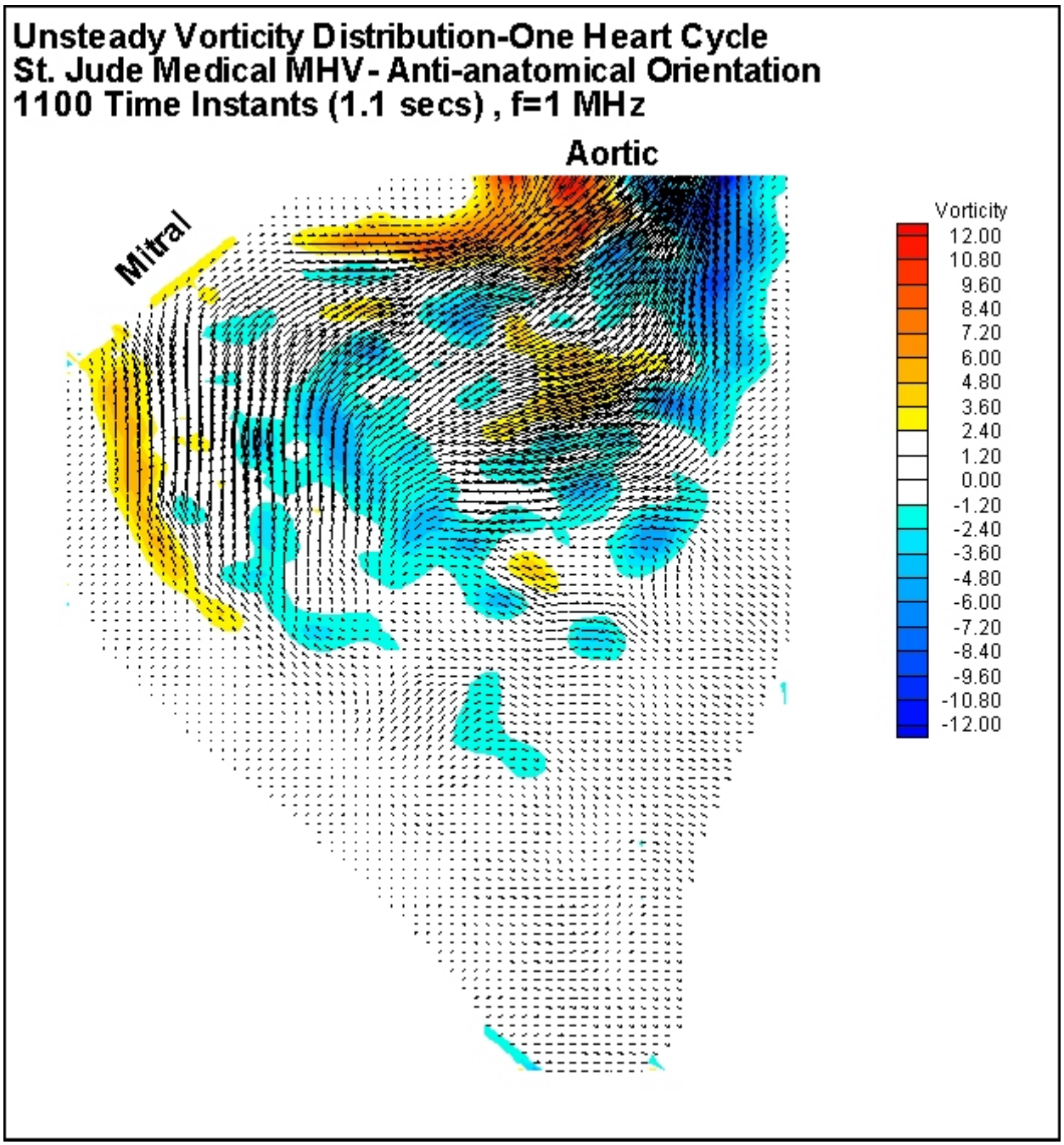

Figure 3.20: Time-varying vorticity and velocity distributions for T = 0.43 secs for the anti-anatomical orientation.

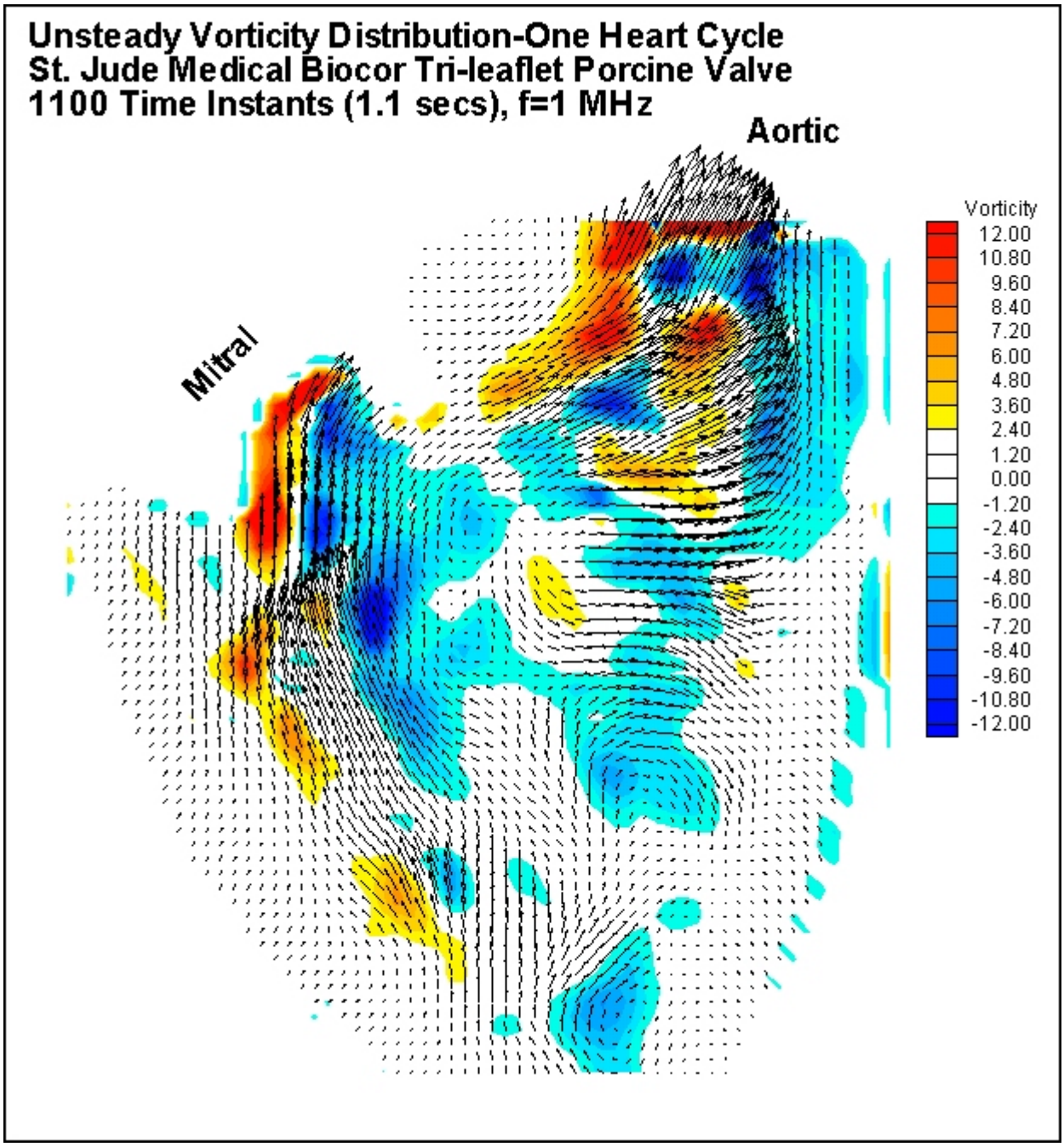

Figure 3.21: Time-varying vorticity and velocity distributions for T = 0.43 secs for the porcine configuration.

In addition, by careful observation of the complete data set, we deduce that during the beginning of diastole T = 0.63 secs, Figures 3.22, 3.23, and 3.24, regurgitation occurs systematically, for the two orientations of the MHV, Figures 3.22 and 3.23, generating small-scale structures in the LV that are present in the domain during the initiation of the diastolic part (T = 0 secs) of the cycle. This feature combined with the large ring vortices that form during the opening of the mitral valve enhance the turbulent characteristics in the flow, increasing the losses inside the LV and, thus, compromising its performance. Furthermore, regurgitation is more pronounce for the anatomical configuration when compared to the anti-anatomical case. Additionally, AV regurgitation in the case of the porcine configuration, Figure 3.24, is not evident. Another observation during this time instants pertains to the MV inlet jet. The incoming jet is asymmetric in the case of the anatomical orientation with the anterior orifice or the one closest to the AV being stronger. For the anti-anatomical and porcine case, the inlet jet is symmetric and more coherent.

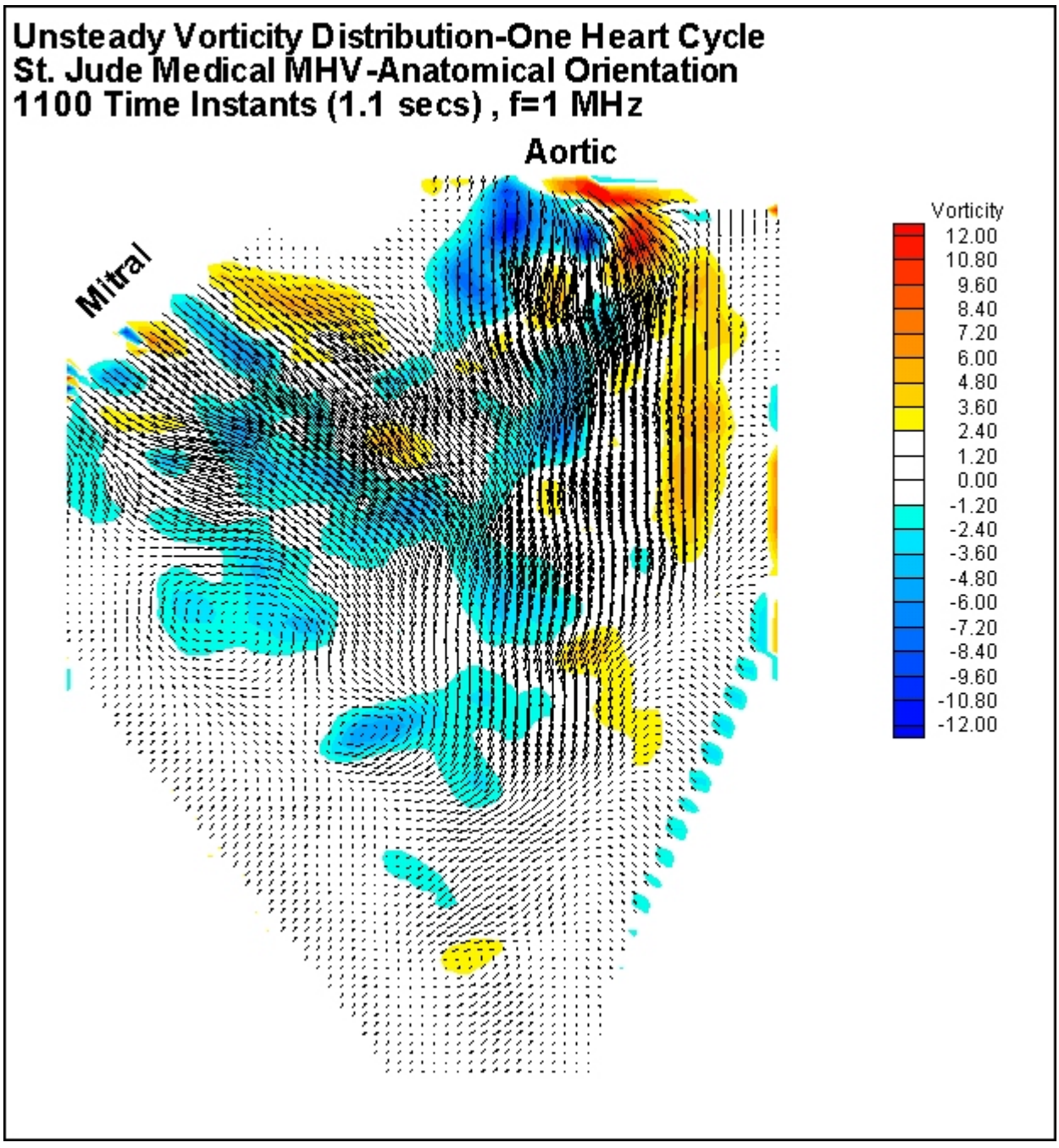

Figure 3.22: Time-varying vorticity and velocity distributions for T = 0.63 secs for the anatomical orientation.

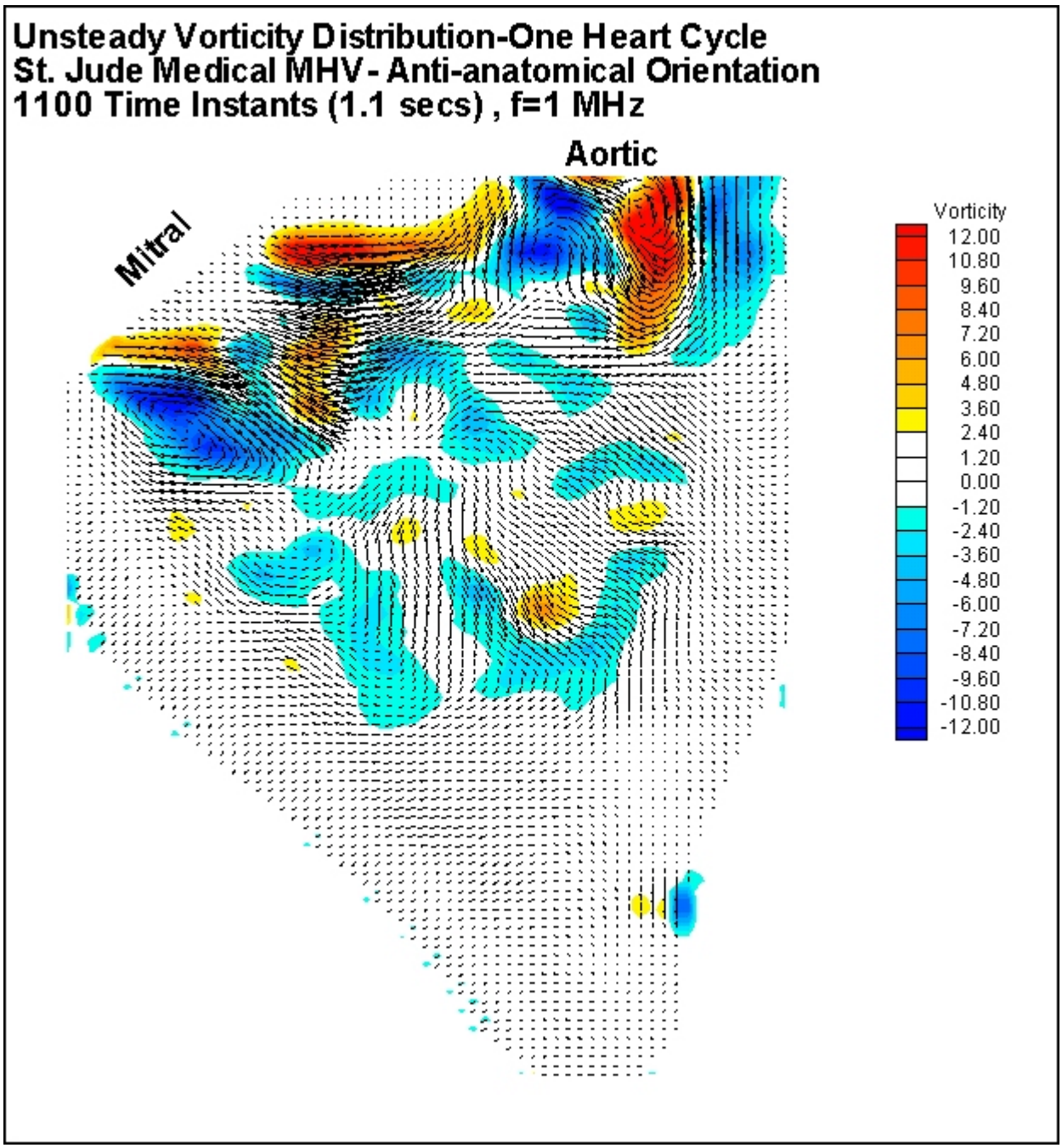

Figure 3.23: Time-varying vorticity and velocity distributions for T = 0.63 secs for the anti-anatomical orientation.

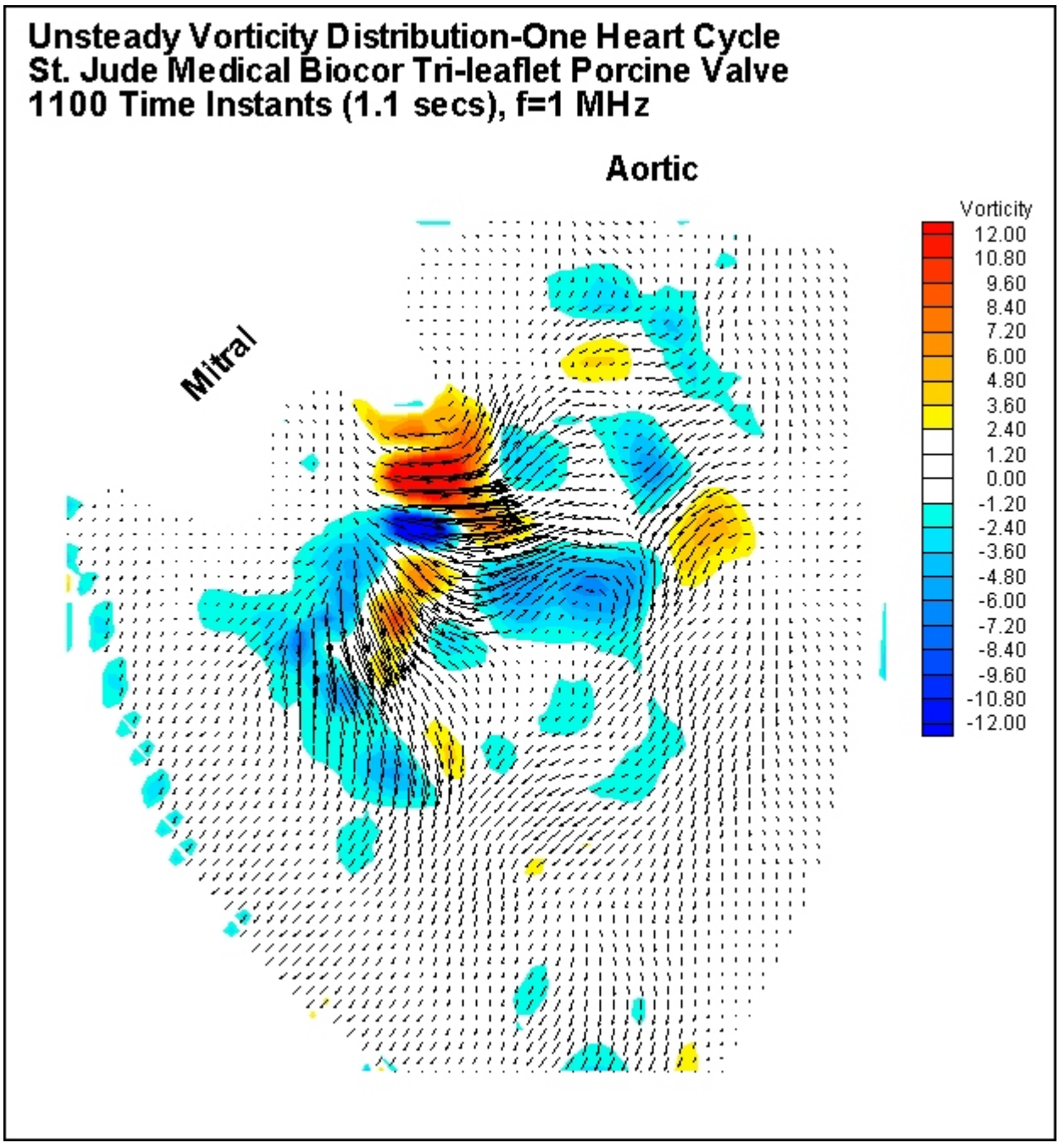

Figure 3.24: Time-varying vorticity and velocity distributions for T = 0.63 secs for the porcine configuration.

The results presented above correspond to sampling frequencies two orders of magnitude higher than the average heart beat rate and with a space resolution of approximately 2% of the mitral valve diameter. This sequence demonstrates, the formation of coherent vortical structures, their evolution and the generation of a turbulent flow field. The intricacy of flow field becomes apparent, illustrating the need for elaborate and detailed analysis of the fluid dynamics inside the left ventricle. High turbulence levels are associated with significant loss of energy and less efficient operation of the heart. It appears that although the natural operation of the heart is energy preserving (as it was discussed in section 1.3.2), the interaction of the fluid with the rigid walls of the mechanical heart valves result into a less efficient mode of operation. This fact indicates that turbulence characteristics of the flow play an important role and only with a measurement technique that provides high sampling frequency and detailed space resolution, the characteristics of the flow can be accurately analyzed. The DPIV system meets these requirements.

Consequently, it is clear that both time averaged and time varying results serve to illustrate some important observations and comparisons between the three cases. From the velocity, vorticity, and turbulent kinetic energy distributions, the presence and location of vortical structures can be deduced as well as the level of coherence of these structures. The detail provided by the entire DPIV system and experimental setup was heretofore unknown from previous studies.

Chapter 4

4 CONCLUSION AND FUTURE WORK

High frequency planar velocity measurements inside the LV were performed using DPIV in order to investigate the effect of MHV orientation on the flow structures. Instantaneous and time averaged flow properties were presented providing an unprecedented wealth of information. Flow patterns that are attributed to the typical three-jet flow generated through a bileaflet MHV generate vortex shedding.

4.1 Mechanical Orientations vs. Porcine Configuration

Investigation of the three cases, anatomical, anti-anatomical and porcine, was conducted so as to see the flow patterns that are enhanced by the distinct orientation of the valve and in turn to compare all three configurations. With a sampling frequency of 1 KHz and spatial resolution in the order of 0.5 mm, we were able to identify vortical structures that survived the end of the systolic phase, which were then trapped in the ventricle and interacted with the new infusion of flow during the following systolic motion. Large amounts of kinetic energy are directed in these vortices. This energy can never be recovered. These results also provide evidence that the level of turbulence is high, which is not present under normal physiological conditions. Specifically, the results show that higher vorticity, turbulence, and vortex intensity levels are evident in the case of the anatomical orientation when compared those of the anti-anatomical and porcine cases. These findings provide a possible explanation of the correlation between the efficiency of the LV and the orientation of the MHVs. This dependence of efficiency to orientation can be attributed to the turbulent character of

the flow and the presence of strong intermittent vortical structures, which are documented in the results. Mitral valve replacement induces a severe alteration of the mechanical environment in the LV, thus, generating flow patterns that are not present under physiological operating conditions, which in return affect the efficiency of the LV.

The presence of three distinct flow patterns was identified for the three configurations, anatomical, anti-anatomical, and porcine, corresponding to significant differences in the turbulence level distribution inside the LV. As was expected, the porcine case has a better overall hemodynamic performance and when comparing the two mechanical orientations, the anatomical orientation has higher vorticity and turbulent kinetic energy levels. One issue involving the vorticity levels and vortical structures present with all orientations pertains to the wake of the valve and the direct relationship the shear regions have on platelet activation. In addition, turbulence increases the collision rate and contact between potentially activated platelets (Bluestein, 2000). Specific regions within the LV for each orientation can be revealed from the present results emphasizing the inherent compromise of both platelet structure and ventricular performance.

4.2 Future Work

While the two-dimensional planar approximation is a viable model for the intricate dynamics of valve orientation, future work and continuing analysis of the data is under way to further establish the three-dimensionality of the flow characteristics inside the LV. This work represents an ongoing effort to qualitatively and quantitatively investigate the flow characteristics inside a flexible transparent LV and downstream of MHVs by employing DPIV. The performance of the heart after a valve replacement operation will greatly depend on the flow character downstream of the mitral valve thus a better understanding of the flow character is essential. Valve orientation during MHV implantation should be of a major concern for the cardiothoracic surgeon. Finally, although the future may lead to innovative valve designs, the challenge today still involves

MHV design optimization, whether that be tilting or orientation of current designs. Additionally, I would like to be able to simulate diseased and exercise conditions in the heart.

Future work will produce data along parallel planes, essentially creating a three-dimensional velocity field in the ventricle. I will extend the measurements to multiple planes and more orientations, specifically more inclinations of the orientation angle for the case of the St. Jude Medical mechanical bileaflet valve. Particular attention will be paid to the immediate neighborhood of the valve leaflets. This will require special optical arrangements to capture the details of the flow during the opening and the closing of the leaflets. Indeed, the flow visualizations indicate that the transient processes of closing and opening are very short. To obtain in greater detail the flow around the leaflets during their dynamic motion, we will need high camera frame rates and detailed spatial resolution. The tools discussed in Chapter 2 will allow us to magnify the regions near the edges of the valves. We will be able to resolve a region of a few square millimeters with the resolution of 512x512 pixels.

Furthermore, as was the case in this present study, processing of the images involved a fixed boundary, which was determined by the maximum size of the left ventricle during the end-diastolic phase. This fixed boundary was implemented through Visiflow, the commercially available package discussed in Section 2.5.1, and certainly that is one limitation of the software, which should be overcome. The hope in the future is to be able to process the images with a dynamically changing boundary. This would allow for better visualization in the vicinity of the changing wall geometry and shear stress gradients could be resolved.

Acknowledgements

Special thanks to St. Jude Medical, who donated the mechanical and porcine valves used for testing and analysis.

REFERENCES

Adrian, R. J., 1991, "Particle-Imaging Techniques for Experimental Fluid Mechanics," ARFM, Vol. 23, pp. 261-304.

Bellhouse, B.J., 1976, Fluid Mechanics of a Model Mitral Valve. The Mitral Valve. A Pluridisciplinary Approach (Edited by Kalmanson, D.), pp99-110.

Bellhouse, B. J., 1972, ``Fluid Mechanics of a Model Mitral Valve and Left Ventricle," *Cardiovasc. Res.*, **6**, pp. 199-210.

Bellhouse, B.J. and F.H. Bellhouse, 1969, "Fluid Mechanics of the Mitral Valve," *Nature*, Vol 224, pp. 615-616.

Bergel, D.H., 1972, Cardiovascular Fluid Dynamics. New York: Academic Press.

Bluestein, D., Rambod, E., and Gharib, M., April 2000, "Vortex Shedding as a Mechanism for Free Emboli Formation in Mechanical Heart Valves," J. Biomech. Eng., Vol. 122, pp. 125-134.

Bluestein, D., and S. Einav., November 1994, "Transition to Turbulence in Pulsatile Flow Through Heart Valves-A Modified Stability Approach." ASME Journal of Biomechanical Engineering. Vol. 116. pp. 477-482.

Bruss, K. H., Reul, H., Van Gilse, J., and Knott, E., 1983, "Pressure Drop and Velocity Fields at Four Mechanical Heart Valve Prostheses: Bjork-Shiley Standard, Bjork-Shiley Concave-Convex, Hall-Kaster and St-Jude Medical," Life Support System, Vol. 1, pp. 3-22.

Chandran, K. B., Schoephoerster, R., and Dellesperger, K. C., 1989, "Effect of Prosthetic Mitral Valve Geometry and Orientation on Flow Dynamics in a Model of Human Left Ventricle," *J. Biomechanics*, Vol. 22, No. 1, pp. 51-65.

Chandran, K. B., Khaloghi, B., and Chen, C. J., 1985, "Experimental Study of Physiological Pulsatile Flow Past Valve Prostheses in a Model of Human Aorta: I. Caged Ball Valves," *J. Biomechanics*, Vol. 18, No. 10, pp. 763-772.

Chandran, K. B., Cabell, G. N., Khalighi, B., and Chen, C. J., 1983, "Laser Anemometry Measurements of Pulsatile Flow Past Aortic Valve Prostheses," *J. Biomechanics*, Vol. 16, No. 10, pp. 865-873.

Fontaine, Arnold A., He Shengqiu, Stadter, Robbie, Ellis, Jeffrey T., Levine, Robert A., Yoganathan, Ajit P., March 1996, ``In Vitro Assessment of Prosthetic Valve Function in Mitral

Valve Replacement with Chordal Preservation Techniques," *J. Heart Valve Dis.*, Vol. 5, No. 2, pp. 186-198.

Garitey, V., Gandelheid, T., Fusezi, J., Pelissier, R., and Rieu, R., 1995 "Ventricular Flow Dynamic Past Bileaflet Prosthetic Heart Valves," *Int. J. Artificial Organs*, Vol. 18, No. 7, pp. 380-391.

Giersiepen, M., Reul H., Knoch, M., and Rau, G., 1986, "Pressure Drop and Velocity Fields at Mechanical Heart Valves," Life Support System, Vol. 4 (suppl 2) pp. 166-168.

Giersiepen M., Krause U., Knott E., Reul H., Rau G., (1989) "Velocity and Shear Stress Distribution Downstream of Mechanical Heart Valves in Pulsatile Flow." *Int J. Artif Organs*, Vol. 12, no. 4, pp. 261-269.

Gross, J.M., Shermer, C.D. and Hwang, H.C. 1988, "Vortex Shedding in Bileaflet Heart Valve Prosthesis" *Vol. XXXIV Tran.Am.Soc.Artif. Intern. Organs*, Vol. 34, pp. 845-850.

Hanle DD, Harrison EC, Yoganathan AP, Alens, DT, Corocran WH. 1989. "In Vitro Flow Dynamics of Four Prosthetic Aortic Valves: a Comparative Analysis." *J. Biomechanics*; 22, 6/7:597-607.

Hasselin L., 1989, "Digital Image Processing in Flow Visualization," ARFM, Vol. 20, pp. 421-485.

Hasenkam JM, Westphal D, Wygaard H, Reul H, Giersiepen M, Stodkilde-Jorgensen H. 1988. "In vitro stress measurements in the vicinity of six mechanical aortic valves using hot-film anemometry in steady flow." *J. Biomechanics*; 21, 3:235-47.

Huang, H. T. and Gharib, M., 1993, "Processing Error in Digital Particle Image Velocimetry." FEDSM97-3068.

Iwase, Hidehito,Liu, Hao, Fujimoto, Shinichi, and Himeno, Ryutaro, November 2001, ``Numerical Analysis of Blood Flow in a Left Ventricle," IMECE2001/BED-23113, Proceedings of 2001 ASME International Mechanical Engineering Congress and Exposition, New York, NY.

Kilner, P.J., Yang, G.-Z., Wilkes, A.J., Mohladin, R.H., Firmin, D.N., and Yacoub, M.H., 2000, "Asymmetric Redirection of Flow Through the Heart," Nature, Vol. 404, pp.759-761.

Kleine P., M. Perthel, J.M. Hasenkam, H. Nygaard, S. B. Hansen, J. Laas, 1999, "High-Intensity Transient Signals (HITS) as a parameter for Optimum Orientation of Mechanical Aortic Valves," *Thorac Cardiov Surg*, Vol. 48, pp. 360-363.

Laas, J., M. Perthel, A. Aiken, and D. Kivelitz, 2000, "Intraventricular Flow in the Normal Heart and After Mitral Valve Replacement," Kurt Singel Mann, Videostudio MHH.

Laas Joachim, Kleine Peter, Hasenkam Michael J., Nygaard Hans, 1999, "Orientation of Tilting Disc and Bileaflet Aortic Valve Substitutes for Optimal Hemodynamics, " *Annals Thorac Surg*, Vol. 68, pp. 1096-9.

Lee, C. S. F., and Talbot, L., 1979, ``A Fluid Mechanical Study of the Closure of Heart Valves," *J. Fluid Mech.*, 91, pp. 41-63.

Lim, W. L., Chew, Y. T., Chew, T. C. and Low, H. T., 1994, ``Particle Image Velocimetry in the Investigation of Flow Past Artifical Heart Valves," *Annals of Biomedical Engineering*, Vol. 22, pp. 307-318.

Liu, J. S., Lu, P. C., and Chu, S. H., 1996, "Pulsatile Flow Past Bileaflet Aortic Valve Prostheses," *J. Chin. Inst. Eng.*, Vol. 19, pp. 333-344.

Mouret, F., Garitey, V., Gandelheid, T., Fuseri, R., and Rieu, R., 2000, "A New Dual Activation Simulator of the Left Heart Which Reproduces Physiological and Pathological Conditions," Medical and Biological Engineering and Computing, Vol. 38, pp. 558-561.

Reul, H., Giersiepen, M., Schindehutte, H., Effert, S., and Rau, G., 1986, "Comparative in vitro Evaluation of Porcine and Pericardial Bioprostheses." Z Kardiol, Vol. 75 (suppl 2), pp. 223-31.

Reul, H., Talukder, N. and Müller, E. W.,1981, ``Fluid Mechanics of the Natural Mitral Valve," *J. Biomechanics*, Vol. 14, No. 5, pp. 361-372.

Schoephoerster, R. T., Oynes, F., Numez, H., Kapadvanjwala, M., and Dewanjee, M. K., 1993, "Effects of Local Geometry and Fluid Dynamics on Regional Platelet Deposition on Artificial Surfaces," *Arterioscler. Thromb.*, Vol. 12, pp. 1806-1813.

Shim, E.-B., and K.-S. Chang., Feb. 1997, "Numerical Analysis of Three-Dimensional Bjork-Shiley Valvular Flow in An Aorta", *ASME Journal of Biomechanical Engineering*, Vol. 119, pp. 45-51.

Shortland, A. P., Black, R. A., Jarvis, J. C., Henry, F. S., Iudicello, F., Collins, M. W., and Salmons, S., 1996, ``Formation and Travel of Vortices in Model Ventricles: Application to the Design of Skeletal Muscle Ventricles," *J. Biomech.*, Vol. 29, No. 4, pp. 503-511.

Sonnenblick, Edmund H., and Robert C. Schlant, 1994, "Normal Physiology of the Cardiovascular System", The Heart, 8th Ed. Vol. 1, pp. 37-63.

Takatsjuji, H., Mikami, T., Urasawa, K., Teranishi, J.-L., Onozuka, H., Takagi, C., Makita, Y., Matsuo, H., Jusuoka, H., and Kitabatake, A., February 1996, ``A New Approach for Evaluation of Left Ventricular Filling Flow Propagation by Color M-Mode Doppler Echocardiography," *J. Am. Coll. Cardiol.*, Vol. 27, No. 2, pp. 365-371.

Tonietto G, 1990, "Etude experimentale et numerique des ecoulements post-valvulaires." These de Doctorat, Universite. Aix-Marseille II, Institut de Mecanique des Fluides de Marseille.

Westerweel J., 1993, Digital Particle Image Velocimetry, Theory and Application. Delft University Press.

Willert C. E., and Gharib, M., 1991, "Digital Particle Image Velocimetry," Experiments in Fluids, Vol. 10, pp. 181-193.

Woo, Y., and Yoganathan, A. P., 1986, "In vitro Pulsatile Flow Velocity and Shear Stress Measurements in the Vicinity of Mechanical Mitral Heart Valve Prostheses," J. Biomechanics, Vol. 19, No. 6, pp. 39-51.

Yoganathan, Ajit P., Ellis, Jeffrey T., Healy, Timothy M., Chatzimavroudis, George P., 1998, ``Fluid Dynamic Studies for the Year 2000," *The Journal of Heart Valve Disease*, Vol. 7, No. 2, pp. 130-139.

Yoganathan, A.P, 1994, "Cardiac Valve Prosthesis" in The Biomedical Engineering Handbook, ed. J.D.Bronzino, pp.1847-1870.

Yoganathan, A. P., Woo, Y., and Sung, H., 1986, "Turbulent Shear Stress Measurements in the Vicinity of Aortic Heart Valve Prostheses," J. Biomechanics, Vol. 19, No. 6, pp. 433-442.

VITA

Olga Pierrakos was born in Sparta, Greece on October 27, 1978. She is the second of four children in the Pierrakos family with two amazing parents, Vasileios and Magdalene. She arrived in the United States at the age of 10 on July 22, 1988, marking a new beginning in her life filled with many challenges and great triumph. Olga resided in Richmond, Virginia where she went to Mills E. Godwin High School and graduated in the top 5% of her class. Olga started her university career at Virginia Tech during the Fall of 1996 at the age of 17. Starting of her undergraduate career as a biology major, she transferred into engineering her sophomore to pursue a more practical, ingenious, and challenging degree. Olga joined the Department of Engineering Science and Mechanics (ESM) to pursue a biomedical engineering concentration. She graduated December of 2000 Magna Cum Laude with her Bachelor of Science Degree in ESM. After much work and intense anticipation, on November 15, 2002, she defended her Master of Science Degree in Engineering Mechanics. Only God knows what the future holds for Olga, but she is eager to conquer new challenges, one of them being a Doctor of Philosophy Degree here at Virginia Tech in the new School of Biomedical Engineering.

"All men by nature desire knowledge."

Aristotle

"You'll come to learn a great deal if you study the Insignificant in depth."

Odysseus Elytis
1979 Nobel Laureate in Literature

"The important thing is not to stop questioning."

Albert Einstein